

1 A new inventory of High Mountain Asia surging glaciers derived from 2 multiple elevation datasets since the 1970s

3 Lei Guo¹, Jia Li¹, Amaury Dehecq², Zhiwei Li¹, Xin Li³, Jianjun Zhu¹

4 ¹School of Geo-science and Info-physics, Central South University, Changsha, 410083, China.

5 ²Univ. Grenoble Alpes, IRD, CNRS, Grenoble INP, IGE, Grenoble, 38000, France.

6 ³Institute of Tibetan Plateau Research, Chinese Academy of Sciences, Beijing, 100101, China.

7

8 *Correspondence to:* Jia Li (lijia20050710@csu.edu.cn)

9 **Abstract.** Glacier surging is an unusual ~~undulation~~instability of ice flow and complete surging glacier inventories are important
10 for regional mass balance studies and assessing glacier-related hazards. Glacier surge events in High Mountain Asia (HMA)
11 are widely reported. However, the completeness of present inventories of HMA surging glaciers is constrained by the
12 insufficient spatial and temporal coverage of glacier change observations, or by the limitations of the identification methods.
13 In this paper, we established a new inventory of HMA surging glaciers based on the glacier surface elevation changes and
14 morphological changes over four decades. Four kinds of elevation sources (KH-9 DEM, NASADEM, COP30 DEM, HMA8m
15 DEM), three elevation change datasets, and long-term Landsat image series were utilized to ~~aeecess~~assess the ~~distinctive change~~
16 ~~patterns~~presence of ~~surging glaeiers during typical surge features over~~ surging glaciers during typical surge features over two time periods (1970s-2000 and 2000-2020). In total
17 890 surging and 336 surge-like glaciers were identified in HMA. Compared to the previous surging glacier inventories in
18 HMA, our inventory incorporated ~~more new~~253 previously unidentified surging glaciers. The number and area of surging
19 glaciers accounted for ~2.49% (excluding glaciers less than 0.4 km²) and ~16.59% of the total glacier number and glacier area
20 in HMA, respectively. Glacier surges were found in 21 of the 22 subregions of HMA (except for the Dzhungarsky Alatau),
21 however, the density of surging ~~glaeier~~glaciers is highly uneven. Surging glaciers are common in the northwest subregions
22 (e.g., Pamir and Karakoram), but scarce in the peripheral subregions (e.g., Eastern Tien Shan, Eastern Himalaya, and Hengduan
23 Shan). The inventory further confirmed that surge activity is more likely to occur for glaciers with larger area, longer length,
24 and wider elevation range. Among the glaciers with similar area, the surging ones usually have steeper slope than the non-
25 surging ones. Besides, we found a potential relationship between the surging glacier concentration and regional glacier mass
26 balance. The subregions with slightly negative or positive mass balance hold large clusters of surging glaciers, while those
27 with severe glacier mass loss hold very few surging glaciers. The inventory and elevation change products of identified surging
28 glaciers is are available at: <https://doi.org/10.5281/zenodo.7590838>~~https://doi.org/10.5281/zenodo.7486614~~ (Guo et al., 2022).
29 **Key words:** High Mountain Asia, Surging glacier inventory, elevation change, KH-9, Digital Elevation Model (DEM)

30 1 Introduction

31 A surge is a glacier instability that translates into an abnormally fast flow over a period of a few months to years (Cogley et
32 al., 2011). A surging glacier exhibits an active phase (surge) and a quiescent phase that may occur at quasi-periodic intervals
33 (Jiskoot, 2011). While a glacier enters into the surging states, a large volume of ice mass is transported downstream at a higher-
34 than-average speed. In the ~~quiescenee~~quiescent phase, a glacier ~~stores~~returns to ~~thea~~ slow-moving ~~status~~against~~state~~, and
35 gradually regains mass ~~at~~in upper recaches. Previous studies pointed out that the surge-type glaciers only ~~eeoccupy~~represent ~1%
36 of total glaciers (Jiskoot, 2011; Sevestre and Benn, 2015). However, glacier surges are far more than an occasional behavior
37 in some specific regions, such as the Alaska-Yukon (Clarke et al., 1986), Svalbard (Jiskoot et al., 2000; Farnsworth et al.,
38 2016), and Karakoram-Pamir (Bhambri et al., 2017; Goerlich et al., 2020; Guillet et al., 2022). Glaciers in these regions have
39 experienced heterogeneous mass loss in the past decades (Hugonnet et al., 2021). How glacier surge activities impact the

40 glacier regional mass balance needs further investigation, and to facilitate this kind of study, the glacier surges needed to be
41 found out first.

42 In recent years, substantial efforts have been made to ~~access~~understand the ~~internal governing rules~~mechanisms of glacier
43 surges, including the hydrological-control(Kamb, 1987; Fowler, 1987), thermal-control(Fowler et al., 2001; Murray et al.,
44 2003), environmental factor(Hewitt, 2007; Van Wyk de Vries et al., 2022), friction state(Thøgersen et al., 2019; Beaud et al.,
45 2021), and the unified enthalpy balance model (Sevestre and Benn, 2015; Benn et al., 2019). To support such studies, the
46 accurate description of surging glacier distribution is needed to provide samples for studying the internal dynamic process of
47 surges. Besides, glacier surge can induce several kinds of hazards, e.g., glacier lake outbursts (GLOF) (Round et al., 2017;
48 Steiner et al., 2018), mudslides (Muhammad et al., 2021), or ice collapse (Kääb et al., 2018; Paul, 2019). Such mountain
49 hazards have been frequently reported in recent decades (Shugar et al., 2021; An et al., 2021; Kääb et al., 2021). A complete
50 inventory of surging glaciers is a basis for the regional hazard assessment of glacier surges.

51 Generally, a surging glacier could exhibit either one or several drastic changes, including: extreme speed-up (by a factor
52 10~1000 compared to normal conditions), distinct elevation change pattern, rapid terminus advance, and surface
53 morphological changes (medial or looped moraine, crevasses, etc.) (Jiskoot, 2011). The identification of surging glaciers can
54 be implemented based on the observation of the above changes, e.g., glacier surface morphology (Clarke et al., 1986; Paul,
55 2015; Farnsworth et al., 2016), terminus position (Copland et al., 2011; Vale et al., 2021), or glacier motion (Quincey et al.,
56 2011). As for the surge-type glacier, which refers to the glacier that possibly surged ~~before~~prior to the observation period, are
57 generally identified by the indirect morphological evidence (without observed changes) (Goerlich et al., 2020). The visual
58 interpretation of glacier surface morphological changes is easy to operate, but fraught with uncertainty due to the snow cover
59 or the absence of supraglacial moraine (Jacquemart and Cicoira, 2022). To recognize abnormal changes in glacier motion, a
60 long-term flow velocity time series is needed (Yasuda and Furuya, 2015; Round et al., 2017). Since the quiescent phase may
61 last for decades and the image source for estimating the flow velocity is limited, the abnormal changes in glacier motion are
62 prone to be missed. By contrast, the recognition of abnormal surface elevation changes is an effective way to identify the
63 surging glaciers, which has been confirmed by several glacier mass-balance studies (Bolch et al., 2017; Zhou et al., 2018), as
64 its source datasets can satisfy the requirement of spatial-temporal coverage with comparatively fewer acquisitions. By
65 combining observations of multiple features, the identification of surging glaciers could be more efficient and complete
66 (Mukherjee et al., 2017; Goerlich et al., 2020; Guillet et al., 2022). However, when conducting such studies on a large spatial
67 scale or a long temporal scale, one should select the least time-consuming but effective identification method. In that case, it's
68 ideal to take the long-term elevation change as the criteria, and to combine with other observations as complements if possible
69 (Guillet et al., 2022).

70 Except for the polar regions, High Mountain Asia (HMA) is the most densely glacierized region in the world. Within the HMA
71 range, several subregions are famous for the concentration of surging glaciers as well as the anomalous glacier mass balance
72 (Hewitt, 2005; Gardelle et al., 2013; Farinotti et al., 2020). The inventories of surging or surge-like glaciers have been
73 established for some subregions like the Karakoram (Bhambri et al., 2017), West-Kunlun (Yasuda and Furuya, 2015), Pamir
74 (Goerlich et al., 2020), Tien Shan (Mukherjee et al., 2017; Zhou et al., 2021). Sevestre and Benn (2015) presented the first
75 global surging glacier inventory by reanalyzing historical reports from 1861 to 2013. However, it was compiled from various
76 data sources (publications, reports, etc.) with inconsistent spatial-temporal coverage, which makes it difficult to ensure
77 accuracy and completeness. Vale et al. (2021) identified 137 surging glaciers across HMA by detecting surge-induced terminus
78 change and morphological changes from Landsat images from 1987 to 2019. The number is obviously underestimated, because
79 it is smaller than the numbers of previous subregional inventories (Bhambri et al., 2017; Goerlich et al., 2020). Guillet et al.
80 (2022) presented a new surging glacier inventory of HMA by identifying multiple glacier change features. In total 666 surging
81 glaciers were identified across HMA. However, the glacier change observation period is shorter than two decades (2000-2018),
82 and therefore some surging glaciers with relatively long revisit cycles may be missed.

83 In this study, we aimed to build a new inventory to include more surging glacier within HMA based on glacier surface elevation
84 change observations over four decades. A workflow was developed to obtain the historical glacier surface elevation change
85 from multiple datasets, including the KH-9 DEM (1970s), NASADEM (2000), COP30 DSM (2011-2014), HMA8m DEM
86 (2002-late 2016), and ~~existed~~previously published elevation change datasets. Glaciers in the new inventory were divided into
87 three classes of confidence in surge detection. After that, the elevation change based inventory were further ~~complete~~completed
88 and corrected by the identification of morphological changes in a long-term timeseries ~~morphological feature identification~~
89 ~~based-on~~of Landsat images (1986-2021). Based on the present inventory, the distribution and geometric characteristics of
90 surging glaciers within HMA were statistically analyzed, in order to demonstrate their spatial heterogeneity and geometrical
91 difference from the normal glaciers.

92 2 Study region

93 High Mountain Asia consists of the Qinghai-Tibet Plateau and the surrounding regions, including the Karakoram, Pamir,
94 Himalayas, and Tien Shan. According to the updated Glacier Area Mapping for Discharge from the Asian Mountains
95 (GAMDAM2) glacier inventory, HMA hosts 131819 glaciers, covering a total area of ~99817 km² (Sakai, 2019). The Hindu
96 Kush Himalayan Monitoring and Assessment Programme (HiMAP) divided HMA into 22 subregions (Fig. 4) (Bolch et al.,
97 2019). Different subregions are influenced by different ~~air-currents~~climate regimes, such as the South Asia monsoon, the East
98 Asia monsoons, and the westerlies (Bolch et al., 2012; Maussion et al., 2014). Glacier mass balance across HMA was found
99 to be heterogeneous in the past decades (Gardelle et al., 2013; Brun et al., 2017; Shean et al., 2020). In particular, glaciers in
100 the Pamir-Karakoram-West Kunlun region had a slightly positive or balanced mass budget (Hewitt, 2005; Zhou et al., 2017;
101 Farinotti et al., 2020), while those in the Eastern Himalayas, Nyainqentanglha and Hengduan Shan mountain ranges
102 experienced substantial ice loss (Maurer et al., 2019).

103 3 Datasets

104 3.1 Elevation Data

105 The NASADEM is mainly reprocessed from the C-band SRTM (Shuttle Radar Topography Mission) images. Among the
106 current global DEMs, the NASADEM has the shortest source data acquisition period (~11/02/2000~22/02/2000) (Farr et al.,
107 2007). Based on an improved production flow, the NASADEM has a better performance than the earlier SRTM void-free
108 product in most regions (Crippen et al., 2016). The NASADEM was employed as the reference elevation source because its
109 acquisition time, 2000, is suitable to divide the elevation change observations to before and after 21st century with moderate
110 time span (one or two decades). Each tile of the product has an extent of 1° × 1° and a pixel spacing of 1 arc-second (see Fig.
111 1a). In total 313 tiles were downloaded from NASA LP DAAC
112 (https://e4ftl01.cr.usgs.gov/MEASURES/NASADEM_HGT.001/).

113 Another global DEM we utilized is the newly released Copernicus DEM GLO-30-DGED (i.e., COP30 DEM). The COP30
114 DEM was edited from the delicate WorldDEM™, which was generated based on the TanDEM-X mission. The global RMSE
115 of COP30 DEM is ± 1.68 m (AIRBUS, 2020). Several studies have pointed out that this DEM is the most reliable open-access
116 DEM to date (Purinton and Bookhagen, 2021; Guth and Geoffroy, 2021). The source images of COP30 DEM were mostly
117 acquired between 2011 and 2014, and therefore COP30 DEM is suitable to represent the surface elevation in the 2010s. Like
118 the NASADEM, the COP30 DEM has a pixel spacing of 1 arc second. Each tile of product has an extent of 1° × 1°. In total
119 313 tiles were downloaded through ESA Panda (<https://panda.copernicus.eu/web/cds-catalogue/panda>).

120 The High Mountain Asia 8-meter DEM (HMA8m DEM) was also utilized in this study. The HMA8m DEM was generated
121 from high-resolution commercial optical satellite stereo images, including WorldView-1/2/3, GeoEye-1, and Quickbird-2

122 (Shean et al., 2020), through an automated photogrammetry workflow that is integrated with multiple error-control processes
123 (Shean et al., 2016). This DEM was originally produced for the mass balance estimation of HMA glaciers, so it covered most
124 of the glacierized regions in HMA. In total 3598 DEM tiles were downloaded from National Snow and Ice Data Center
125 (https://nsidc.org/data/HMA_DEM8m_MOS/versions/1). About 95% of them were acquired between 2010 and 2016 (Fig. 1b).
126 Due to the data voids and inconsistent acquisition time, the HMA8m DEM was taken as a supplementary elevation source to
127 increase the observations in the 2010s.

128 The Hexagon KeyHole-9 (KH-9) imagery was acquired in the 1970s. It is one of the earliest near-global satellite stereo image
129 source. The KH-9 imagery is characterized by a spatial resolution of 6-9 m, a wide coverage (130 km x 260 km), and a 70%
130 forward overlap (Surazakov and Aizen, 2010). Many studies have utilized this imagery to estimate historical glacier surface
131 elevation (Holzer et al., 2015; Zhou et al., 2017; Maurer et al., 2019). The KH-9 DEMs used in this study were generated
132 through the automated ASPy pipeline (Dehecq et al., 2020). The methodology, validated in the European Alps and Alaska
133 achieved a vertical accuracy of ~5m (68% confidence level). For more details on the method of KH-9 DEM generation, please
134 refer to Dehecq et al. (2020). In total 238 DEMs with a resolution of 48 m were generated from the KH-9 images acquired
135 between 1973 and 1980. The KH-9 DEMs were utilized to represent the glacier surface elevation in the 1970s (See Fig. 1c).
136 Several newly published elevation change datasets were also collected to include the most recent surges as much as possible
137 (Brun et al., 2017; Shean et al., 2020; Hugonnet et al., 2021). We mainly used the elevation change results presented by
138 Hugonnet et al. (2021) to extend the observation period to 2020, which has a resolution of 100 m and a temporal interval of 5
139 years. Through the inter-comparison of the multiple elevation change results, the gross errors or false signals in the elevation
140 change patterns could be easily detected.

141 3.2 Optical Satellite Images

142 In order to assist the identification of surging glacier, we also ~~recognized the glacier identified~~ morphological ~~feature~~-changes
143 ~~from associated with surges in~~ multi-temporal optical satellite images. ~~We mainly relied on~~ the 1986-2021 Landsat ~~imageries~~
144 ~~were mainly utilized imagery~~ to capture the glacier morphological changes. We downloaded the false-colour composited
145 Landsatlook images ~~with 30m resolution~~ (geo-referenced) that have good brightness contrast over snow/ice areas from USGS
146 website (<https://earthexplorer.usgs.gov>). The images were pre-selected to satisfy the requirement of cloud cover (<10%). In
147 total, 7843 Landsatlook images in 148 frames were used (see Fig. 1d). We also utilized the very high-resolution (VHR) images
148 (Google/ESRI/Bing, etc.) as complements for surging feature identification. The fine resolution of these images allows us to
149 visually check the possible morphological features caused by past surges.

150 3.3 Glacier inventory

151 In this study, we used the GAMDAM2 glacier inventory (Sakai, 2019) as template for the surging glacier inventory, rather
152 than the Randolph Glacier Inventory V6.0 (RGI6.0) (RGI Consortium, 2017). The GAMDAM glacier inventory has included
153 many small glaciers that are missed in RGI6.0, and provides a more accurate glacier extent by excluding outcrop rocks and
154 shaded areas (Nuimura et al., 2015). Since the GAMDAM2 inventory only contains the glacier polygon vectors, we calculated
155 the geometric and topographic attributes for each glacier in a way similar to that of RGI6.0. The maximum glacier centreline
156 was calculated through the Open Global Glacier Model (OGGM) (Maussion et al., 2019). The attributes were used to interpret
157 the geometric characteristics of surging glaciers.

158 4 Methodology

159 4.1 Estimation of glacier surface elevation change

160 The four kinds of DEMs have different coordinate references, vertical references, and data formats. Firstly, all DEMs were
161 converted to float GeoTiff format. For datasets with quality files (NASADEM and the COP30 DEM), the DEM were
162 preprocessed to mask out the pixels of low quality. The poor pixels of COP30 DEM tile were determined through the attached
163 height error map (with values larger than 2.5 m) and water body map (with values not equal to zero). The NASADEM was
164 directly masked with the attached water mask file. Subsequently, the coordinate system, map projection, and vertical reference
165 of all DEMs tiles were unified as the WGS84 coordinate system, HMA Albers Equal Area projection (Shean et al., 2020), and
166 WGS84 ellipsoid. The glacier surface elevation changes during 2000-2010s were derived by subtracting the NASADEM from
167 the COP30 DEM and HMA8m DEM, and those during 1970s-2000 were derived by subtracting the KH-9 DEM from the
168 NASADEM.

169 An automated DEM differencing workflow for large-scale glacier surface elevation change estimation was developed based
170 on the *demcoreg* package presented by Shean et al. (2019). The workflow integrated multiple DEM co-registration approaches,
171 the polynomial fit of tilt error, and other adaptive outlier removal approaches that was operated based on the observations over
172 stable regions. Hence, a mask that excluded the water bodies and glacierized regions was generated in advance. Before
173 differencing, the two DEMs need to be co-registered, because a small geolocation shift can result in considerable elevation
174 change errors in high mountain regions. The efficient analytical DEM co-registration method presented by Nuth and Kääb
175 (2011) was used to eliminate the relative geolocation shift between DEMs. This method assumes the geolocation shift vectors
176 of all DEM pixels are identical. However, for the global DEM products like NASADEM and COP30 DEM, a DEM tile was
177 usually mosaiced from multiple DEM patches, and the geolocation shift vectors at different parts of the DEM tile may be
178 different. In view of this problem, we developed a block-wise version of the analytical DEM co-registration method to reduce
179 the impacts of geolocation accuracy anisotropy of a DEM tile. Each DEM tile was divided into $m \times n$ blocks, and the DEM
180 shifts were estimated for each block. Then, the $m \times n$ groups of shift parameters were merged into one group of shift parameters
181 through a cubic interpolation. Technically, the estimated shift parameters become increasingly representative as the block size
182 decreases. However, the fitting of shift parameters requires a certain number of samples. The final block size was set to
183 300×300 pixels to reach the best balance between the representativeness and estimation accuracy of shift parameters. Besides,
184 we found that the block-wise co-registration method could result in wrong fitting of shift parameters over flat regions. To deal
185 with this, a threshold of mean slope (10°) was set to classify the DEMs into the flat and the hilly categories, and the original
186 global co-registration method (Nuth and Kääb, 2011) was applied to the flat ones.

187 Due to the residual orbital error of satellite images, the elevation difference maps often showed planimetric trends. This type
188 of systematic error was fitted as a universal surface trend using a quadratic polynomial model based on the observations in
189 stable regions, and then was removed from the elevation difference tile (Li et al., 2017). Besides, due to the jitter of the SAR
190 antenna and optical mapping camera, the elevation difference maps often showed stripes (i.e., band-like artifacts) (Yamazaki
191 et al., 2017). To eliminate the stripes, the elevation difference map was converted to the frequency domain through the Fast-
192 Fourier-Transform method. Since the cyclic values have a high frequency in the power spectral density map, a threshold of
193 frequency was set to separate the stripes components from the normal elevation differences. The de-stripping was completed
194 after the backward transformation. Finally, the outliers of elevation difference maps were reduced through the 3-sigma
195 threshold criteria.

196 The radar penetration into glacier surface can result in biases of elevation change estimation, which could be several to dozens
197 of meters, and potentially can lead to the false positive identification. We adopted a two-step procedure to reduce the radar
198 penetration bias in the final elevation change results. First, we used the DEM differencing workflow mentioned above to
199 ~~minus~~ subtract the NASADEM from the SRTM-X DEM. The elevation differences over glacierized area were regarded as the

200 penetration difference between X-bands and C-bands. Secondly, we fitted a 3rd polynomial function between the glacial dH
201 and altitude, which was deemed as the penetration depth – altitude relationship. Then, the radar penetration biases were
202 removed from the COP30 DEM related results by taking the glacier elevation as input for the function. For the dH results
203 calculated by differencing NASADEM and optical DEMs (e.g. HMA8m and KH-9 DEM), the penetration difference of X-
204 and C- bands was multiplied by 2 to represent the absolute penetration depth of C-band (Abdel Jaber et al., 2019; Fan et al.,
205 2022) and then removed from the related results.

206 Finally, three elevation change maps were calculated: the COP30 DEM – NASADEM, the HMA8m DEM – NASADEM, and
207 the NASADEM – KH-9 DEM. The first two elevation change maps were combined with the three elevation change datasets
208 for surging glacier identification during the period 2000-2020, and the last one during the period 1970s-2000. In total, our
209 elevation change observations covered ~92% of the total glacier area within HMA in 2000-2020, and ~77% in 1970s-2000.
210 Gaps in observations were mainly due to: 1) data voids and incomplete coverage of original DEMs tile, which was the main
211 cause for the KH-9 DEMs and HMA8m DEM related results; 2) gross error removal during the elevation change calculations,
212 which led to the scattered holes in the COP30 DEM related results.

213 4.3 Surging glacier identification

214 The identification of surging glaciers in this study were divided into three steps. First, we generated a raw inventory of surging
215 glaciers through the qualitative interpretation of multi-temporal elevation changes. Then, the visual identification of
216 morphological-**feature** changes was carried out for the identified surging and surge-like glaciers. This procedure can further
217 confirm the surges or correct the false identifications based on glacier elevation changes (Guillet et al., 2022). The identified
218 results were re-checked by careful inspection on VHR images, and by comparing with existed surging glacier inventory. Also,
219 the surging tributaries were separated from the non-surging glacier trunk at this step.

220 4.3.1 Identification through elevation changes

221 In general, a typical glacier surge cycle can be divided into three phases (Jiskoot, 2011): 1) the build-up phase, characterized
222 by remarkable thickening in the upper reaches; 2) the active phase, characterized by remarkable thinning in the upper reaches
223 and thickening in the lower reaches; 3) the post-surge phase, characterized by strong down-wasting in the lower reaches. The
224 classical method of identifying surging glaciers is to recognize the combination of marked upper thinning and lower thickening
225 in the longitudinal direction. However, to distinguish the surging glaciers in the build-up or post-surge phase, careful
226 comparison with surrounding glaciers is required, which is difficult to be carried out with a mathematical index. In this study,
227 we established a three-class indicator to distinguish the surge possibility through the visual interpretation of glacier elevation
228 change patterns:

229 I) “verified”:

- 230 - a) obvious thickening in lower reaches (e.g. +30 m);
- 231 - b) contrasting upper-thinning (e.g. +20 m) and lower-thickening (e.g. +20 m);
- 232 - c) contrasting upper-thickening (e.g. +20 m) and lower-thinning (e.g. -30 m);
- 233 - d) severe thinning in the lower reaches (two time stronger than that of the normal glaciers, or comparable to the
234 ablation of adjacent “verified” surging glaciers);

235 II) “probable”:

- 236 - a) moderate upper thinning (e.g. -15m) and lower thickening (e.g. +15m);
- 237 - b) only moderate thickening in the middle reaches (e.g. +15m);

238 III) “possible”:

- 239 - a) only moderate thickening at the terminus (e.g. +15m);
- 240 - b) only strong thinning in the lower reaches (one time stronger than adjacent normal glaciers).

241 Note that, the specific values of elevation change mentioned above were for information only. Because of the diversity in the
242 regional elevation change patterns under different climate or topographic conditions, the thresholds may vary spatially.
243 The identification of surging glaciers was conducted separately in the two observation periods (1970s-2000 and 2000-2020).
244 The sub-inventory covering the period 1970s-2000 was generated based on the dH results of NASADEM – KH-9 DEM. For
245 the sub-inventory covering the period 2000-2020, its dH datasets contain the COP30 DEM – NASADEM, the HMA8m DEM
246 – NASADEM, and three previously published elevation change datasets (Brun et al., 2017; Shean et al., 2020; Hugonnet et
247 al., 2021). Within each observation period, each glacier will be labelled with its possibility level of surging and elevation
248 change pattern in the attribute table. For example, the label of “I-c” means this glacier was classified as “verified” surging
249 glaciers because contrasting upper-thickening and lower-thinning pattern were observed in the corresponding period. Figure 2
250 shows an example of surging glacier identification result.

251 4.3.2 Identification through morphological ~~feature~~ changes

252 Long-term Landsat images (acquired between 1986 and 2021) were utilized to investigate the morphological ~~change~~
253 ~~features~~ changes of the three types of potential surging glaciers identified from elevation change. With each Landsat image
254 acquisition frame, all Landsatlook images of different dates (acquired from 1986 to 2021) were ~~be~~ merged into an animated
255 time-series image. Based on the animated image, we are able to easily identify the morphological ~~feature~~ changes.
256 ~~Regarding~~ ~~Due to~~ the moderate resolution of Landsat images, only three types of feature changes were utilized as criteria for
257 identifying glacier surges: terminus position change, looped moraine changes, and medial moraine changes. Similarly, we
258 assigned a two-level index to each morphological change to indicate our confidence at the identification, which was defined
259 as follow:

260 1) terminus advance:

261 I) : obvious terminus advancing (e.g. over 500 m);

262 II): small terminus advancing (e.g. 0~500 m);

263 2) looped/medial moraine change:

264 I) : fast formation/vanishment of the looped moraine, or obvious distortion of the medial moraine;

265 II) : slow formation or vanishment of the looped moraine, or slight shape changes of existed looped moraine, or
266 slight distortion of the medial moraine.

267 Each of the three kinds of morphological changes were individually qualified and labelled in the attribute table.

268 4.3.3 Generation of surging glacier inventory

269 Through the above identification steps, in total five indicators were compiled to describe the changes of possible surging
270 glaciers. The two sub-inventories of dH identified results were merge firstly ~~followed~~ ~~following~~ the principle of possibility, i.e.,
271 if a glacier was identified as a surging glacier in both ~~two~~ periods but ~~attached~~ ~~associated~~ with different indicators, its indicator
272 in the final inventory was taken from the indicator having a higher possibility. The possibility of indicators follows the order:
273 “verified” > “probable” > “possible”. For example, a glacier was identified as a “verified” surging glacier in the period 1970s-
274 2000, and was identified as a “probable” surging glacier in the period 2000-2010s, then it was qualified as a “verified” surging
275 glacier. After that, the merged dH indicators were further compared with the morphological indicators to determine the final
276 indicator of surge possibility. The “probable” or “possible” class was changed to a class with higher possibility (e.g., from
277 “probable” to “verified”) only if a “I” kind of morphological change was found.

278 We think the advancing glaciers usually have such features: 1) only thickened in a small area at terminus, without contrasting
279 upper thinning; 2) the advancing distance is relatively short (Lv et al., 2019, 2020; Goerlich et al., 2020). These features are
280 corresponding to the “III-a” type of elevation change, and “II” type of terminus advance. Therefore, if a glacier only shows
281 these two kinds of changes, it will be qualified as an advancing glacier, rather than a surging glacier.

282 For ~~some~~ glacier complexes ~~that only in which a~~ tributary surged ~~while but~~ the main trunk did not show any features of surge,
283 such as the Biafo glacier, Fedchenko Glacier and Panmah Glacier (Hewitt, 2007; Goerlich et al., 2020; Bhambri et al., 2022),
284 it's necessary to separate the surging tributary from the trunk. A tributary will be considered as an individual surging glacier
285 if it has the following features. Firstly, the dividing line transition of contrasting elevation change ~~locates within~~ is located in
286 this tributary. Secondly, the ~~volume of~~ mass contributed by this tributary to the glacier trunk is relatively small. Then we
287 manually edited the outline to separate the tributary from the glacier complex. This kind of surges was also marked by the
288 attribute of "trib_surge".

289 In the final step, we inspected the identified surging glaciers on VHR imagery. The inspection aimed to remove the wrong
290 identification due to some false signals, such as the severe lower-thinning in a lake-~~terminated~~ terminating glacier and
291 remarkable surface heightening caused by nearby landslide. We also refined our inventory ~~through the careful~~ after careful
292 comparison with inventories presented by Guillet et al. (2022), Goerlich et al. (2020) and Bhambri et al. (2017). ~~For the surging~~
293 ~~glaciers that identified in other inventories but not included in ours, we did a careful re-identification.~~

294 **5 Results**

295 **5.1 Identified surging glaciers**

296 A total of 1226 surge-related glaciers across the HMA were identified based on the elevation changes and morphological
297 ~~feature~~ changes. The identified surge-related glaciers consisted of 890 'verified' surging ones, 208 'probable' ones, and 128
298 'possible' ones. A total of 175 surging tributaries were identified in 86 glacier complexes. When merging the identification
299 results of the two periods, we found that a considerable proportion of identified surging glaciers were simultaneously
300 recognized in two periods. This makes our inventory more ~~convincible~~ reliable, since a surging glacier could exhibit different
301 kinds of changes in different periods. For example, 26 probable and 51 possible surging glaciers identified during 2000-2020
302 turned to be "verified" surging glaciers during 1970s-2000. Meanwhile, 60 "probable" and 21 "possible" surging glaciers
303 identified during 1970s-2000 turned out to be 'verified' surging glaciers during 2000-2020. Thanks to an almost complete
304 coverage of the elevation change observations, we were able to classify all glaciers in HMA. Table 1 shows the number of
305 surging glaciers identified from two periods of elevation changes and morphological ~~feature~~ changes. Due to the incomplete
306 coverage and data voids of KH-9 DEMs, fewer surging glaciers were identified during the period 1970s-2000. The "probable"
307 and "possible" classes were deemed as surge-like glaciers. To avoid confusion, only the "verified" surging glaciers were used
308 for analysis and comparison throughout the rest of this study.

309 **5.2 Distribution of surging glaciers**

310 Surging glaciers were identified in 21 subregions of HMA (except for the Dzhungarsky Alatau), however, the density of
311 identified surging glaciers is far from even (Fig. 3). Glacier surges are common in the northwest regions, sporadic in the inner
312 regions, and scarce in the peripheral regions. Figure 4 and Table 2 show the ratios of surging glacier number and area in each
313 subregion. Considering the area of the smallest identified surging glacier is 0.42 km², we only took the glaciers larger than
314 0.40 km² in the glacier number related ratio. When conducting statistical analysis, the surge-like glaciers were ~~not accounted~~
315 ~~in such statistics~~ excluded from the dataset, and a surging tributary was regarded as an individual glacier. The number (890)
316 and area (16556.42 km²) of identified surging glaciers accounted for ~2.49% and ~16.59% of the total glacier number and
317 glacier area in HMA, respectively.

318 Among the 22 subregions, the Karakoram is the largest cluster of surging glaciers. In total 354 surging and 128 surge-like
319 glaciers were identified in the Karakoram. The number and area of verified surging glaciers in the Karakoram accounted for
320 39.80% and 47.90% of the total ~~glacier number and area within HMA. In the Karakoram, identified~~ surging glaciers ~~has~~
321 ~~accounted for 8.59% of the total glacier number, within HMA.~~ We found more than half of the tributary surges (101) occurred
322 in the Karakoram, where large glaciers are much more developed than other regions. ~~The area of~~ In the Karakoram, although

323 surging glaciers have only accounted for 8.59% of the total glacier number, their area occupied 39.48% of the total
324 glacier glacierized area in Karakoram. The Pamirs, composed of the Eastern Pamir, Western Pamir and Pamir Alay, hosts 249
325 surging glaciers and 128 surge-like glaciers. About 27.74% of the glacier area in the Eastern and Western Pamir belongs to
326 surging glaciers. We also found 28 surging tributaries in 15 glacier complexes in the Pamirs. Surging glaciers are also common
327 in the Western Kunlun. In total 82 surging and 47 surge-like glaciers were identified in the West Kunlun, and the area of
328 surging glaciers accounted for 30.48% of the total glacier area. The Central Tien Shan has the fourth largest surging glacier
329 area. In total 59 surging glaciers were identified in the Central Tien Shan, which covered 12.93% of the total glacier area. The
330 Karakoram, Pamirs, West Kunlun, and Central Tien Shan nourished host ~83% of the surging glaciers across HMA. Figure 5
331 shows the distribution of identified surging and surge-like glaciers in these four regions.
332 Within interior HMA subregions (including the Tibetan Interior Mountains, Eastern Kunlun Shan, and Tanggula Shan), the
333 number of identified surging glaciers only covered represents less than 2% of the total glacier number, but the area accounted
334 for near 15% of the total glacial area. Surging glaciers in these regions are generally gathered in some a few watersheds. Similar
335 localized surging glacier clusters were also found in the Nyainqentanglha, Northern and Western Tien Shan, and Central
336 Himalaya, but the corresponding area ratios are much lower. In these regions, our inventory covered dozens of surging glaciers
337 which were rarely reported before. Figure 6 shows some samples of identified surging glaciers in these regions.

338 5.3 Geometric characteristics of surging glaciers

339 In this part, only the surging glaciers and non-surging- glaciers are taken for analysis. The surge-like glaciers are not included.
340 All glacier samples in the surging and non-surging classes are larger than 0.40 km².
341 We divided all glaciers into 9 classes according to their area, and calculated the ratios of surging glacier number and area in
342 each class. As shown in Figure 7, surging glaciers were found in all classes. Both the ratios of surging glacier area and number
343 became increasingly high as the glacier size increased, except for the last class. Surging glaciers with an area of 1~50 km²
344 occupies 82% of all surging glaciers. For the three classes in which glaciers are larger than 50 km², the ratios of surging glaciers
345 area and number were about 52% and 54%, respectively. In particular, 2 of 6 very large glaciers (the Siachen glacier and
346 Hispar glacier) surged during our observation periods.
347 When comparing the geometric characteristics of the surging glaciers and non-surging glaciers, we selected samples in the
348 following way: for each surging glacier, we selected 10 non-surging glacier samples that have closest area; and then we
349 randomly sampled 3 out of the 10 selected non-surging glaciers. This is to minimize the discrepancy resulted from the sample
350 differences. There are two reasons for doing so. First, the gap between the sample numbers is huge (~35000 non-surging vs.
351 890 surging). Second, a high proportion of non-surging glaciers are very small glaciers. The final selected 890×3 non-surging
352 glaciers formed the reference group.
353 We first analysed the distribution of surging glacier number and area in eight orientations. As shown in Fig. 8, both the number
354 and area of glaciers facing the north are the largest, and then followed by those facing the northwest and northeast. The
355 distribution of the glacier orientation in reference group were different than that of the non-surging glaciers, which confirmed
356 the statistical analysis would be affected by sample differences. The number of surging glaciers facing the north accounted for
357 ~30.1% of the total surging glacier number, and their area accounted for ~27.8% of all surging glacier area. The number and
358 area ratios of surging glaciers facing the north are obviously higher than that of the non-surging glaciers facing the north, while
359 the number and area ratios of surging glaciers facing the northwest are obviously lower than that of the non-surging glaciers
360 facing the northwest. Meanwhile, the area ratio of surging glaciers facing the northeast is considerable higher than the number
361 ratio, but for surging glaciers facing the northwest and southwest the situation is opposite.
362 Figure 9 illustrates the comparisons between the basic geometric properties of surging and non-surging glaciers. The sampling
363 strategy mention above was also utilized here. If we directly compare the surging glaciers with all non-surging glaciers, we
364 will find that surging glaciers generally have a larger area, wider elevation range (i.e., the highest glacier surface elevation

365 minus the lowest), and longer flowline (Fig 9a-c). Taking the median values as the candidates, the quantitative comparisons
366 are 7.3 km² (surging) vs. 0.87 km² (non-surging) for glacier area, 1534 m vs. 642 m for elevation range, and 6695 m vs. 1854
367 m for maximum glacier length, respectively. In terms of mean surface slope and median elevation, the values of the surging
368 glaciers are less spread out than the non-surging glaciers. However, the median values of the two kinds of glaciers are very
369 close (see Figures 9d and 9e). If we took the non-surging glaciers in reference group for comparisons, the discrepancies of two
370 kinds of groups on these geometric properties became much more different. As shown in Figure 9a, the similar boxplots of
371 reference group and surging glacier samples proved that our sampling strategy has successfully re-organized the non-surging
372 glacier samples for comparisons. The gaps between the surging and non-surging glaciers (reference group) in the glacier area
373 (7.3 km² vs. 7.0 km²), elevation range (1534 m vs. 1180 m) and glacier length (6695 m vs. 5560 m), are much smaller. More
374 importantly, the mean slope of the glaciers in reference group become smaller than that of the surging glaciers.
375 The correlation between different glacier geometric properties was analysed through the bivariate scatterplots (see Figure 10).
376 Among the glacier area, glacier length, and glacier surface elevation range, any two of them have an apparent positive
377 correlation. The glacier mean slope has a moderate correlation with the glacier area, glacier length, and glacier elevation range.
378 By contrast, the glacier median elevation has little correlation with glacier area, glacier length, glacier elevation range, and
379 glacier mean slope. The correlation of any two geometric properties makes little difference between surging and non-surging
380 glaciers.

381 6 Discussion

382 6.1 Uncertainty analysis

383 The reliability of surging glacier identification is directly related to the accuracy of glacier surface elevation change. Assuming
384 the uncertainties in surface elevation change are similar over glacierized areas and stable areas, we evaluated the glacier
385 elevation change uncertainties based on elevation change observations in stable areas, whose true values are zeros. Meanwhile,
386 the uncertainties in the radar penetration calculation were also considered through the error propagation law. The normalized
387 median absolute deviation (NMAD) is less sensitive to outliers and can be deemed as an alternative to standard deviation
388 (Höhle and Höhle, 2009). Hence, the NMAD was used to denote the uncertainty of individual glacier surface elevation change
389 tile (Li et al., 2017). Figure 11 shows the NMAD of elevation change observations in stable areas within each DEM
390 differencing tile, which were used for the co-registration and biases removal during the glacier elevation change estimation.
391 Due to large distortions in the KH-9 images, the NASADEM - KH-9 DEM results had the highest uncertainties. Benefiting
392 from the advantages of bistatic SAR image pairs, the COP30 DEM has high quality, and the COP30 DEM related results had
393 the lowest uncertainties. The HMA8m DEM related results had moderate uncertainties. The average NMAD of all DEM
394 differencing tiles was smaller than 5 m. The significant elevation errors usually occurred in the highly rugged regions such as
395 crests and horns. The terrain of glacier surface is relatively gentle, and therefore the uncertainties of glacier surface elevation
396 changes should be lower than the estimated values: over the area where surge occur. The top of glaciers usually includes very
397 steep faces and have a lot of uncertainties, but it does not matter too much for this study. In general, the uncertainties of our
398 elevation change results are well-controlled. Compared with the typical surface elevation change ~~resulted~~resulting from a
399 glacier surge (tens to hundreds of meters), the magnitudes of uncertainties are very small.
400 Similar to previous studies (Sevestre and Benn, 2015; Goerlich et al., 2020), the surging glacier identification in this study
401 was completed through a manual qualitative interpretation ~~way~~. It's difficult to provide a quantitative index to represent
402 the uncertainty of surge identification. However, the four-class indicator of surge likelihood could aid that in a degree.

403 6.2 Characteristics of surging glaciers

404 The direct comparisons between geometric characteristics of surging and non-surging glaciers manifest that surge activity is
405 more likely to occur in the glacier with a larger area, wider elevation range, and longer length (Fig. 9). Previous studies also
406 reported this phenomenon (Barrand and Murray, 2006; Jiskoot, 2011; Sevestre and Benn, 2015; Mukherjee et al., 2017; Guillet
407 et al., 2022). Larger area, wider elevation range, and longer length mean a larger glacier scale and more mass storage. Surge
408 is a self-balancing process of a glacier to regulate its internal instability of thermal or hydrologic conditions which needs
409 enough mass storage. In this case, about 97% of the surging glacier has an area ~~of~~ larger than 1 km². For glaciers larger than
410 10 km², surge becomes a quite common behavior (with a number ratio higher than 20%), rather than an accidental behavior
411 (see Fig.7).

412 In terms of mean surface slope, we could not observe a statistically difference in the median value of the surging and non-
413 surging glaciers, although the surging glaciers have a more concentrated value range (Fig 9d and Figure 10, 3rd row, 1st
414 column). After minimizing this kind of bias, we observed an obvious higher mean slope of surging glaciers in the comparison
415 with the reference group. Several studies have demonstrated that the surging glacier tend to have shallower slope (Jiskoot et
416 al., 2000; Guillet et al., 2022). However, here we reasonably argue that this rule was concluded from an unbalanced comparison,
417 as ~~the non-surging glaciers are consist of much larger~~ have a higher proportion of small glaciers than surging glaciers ~~does~~.
418 Meanwhile, the inverse relationship between the glacier slope and length (Clarke, 1991; Sevestre and Benn, 2015) may not
419 apply to very small glaciers (i.e. smaller than 1 km²). As shown in Fig. 9d and Fig. 10, among the non-surging glaciers, the
420 small ones occupy a high proportion and their mean slope presents strong variability. Regarding this, we can conclude that
421 steeper glaciers are more likely to surge when the comparison is restricted to similar areas. ~~Considering the fact that steeper~~
422 ~~valley glaciers are more prone to reach the crucial gravitational imbalance, this conclusion should be reliable.~~ As for the glacier
423 median elevation, since it is almost irrelevant to the glacier area, glacier length, glacier elevation range, and glacier mean slope
424 (see Fig. 10), it can be deemed as an irregular glacier index. However, among glaciers that have similar areas, steeper glaciers
425 generally have lower median elevation. That's why the median elevation of surging glaciers is slightly smaller than that of
426 non-surging glaciers (Fig. 9e).

427 These comparisons could now lead to a conclusion as follows: the surging glaciers are generally longer, and have larger
428 elevation ~~spanning range~~ than non-~~leapfrogsurging~~ glaciers, since they have more mass storage. However, when glaciers are
429 similar in area, a steeper surface slope is more likely to lead to surge.

430 Besides, our results ~~manifested~~ highlights that the ratio distribution of surging glaciers in eight aspects are slightly different
431 from that of non-surging glaciers (see Fig. 8). ~~This is in line with the findings in previous studies. In particular~~ Overall, the
432 ratio of surging glaciers is relatively higher than the non-surging glaciers in the north ~~direction and northeast directions~~, but
433 lower in the northwest direction. ~~This is mainly caused by the orientation of the mountains in Karakoram and Pamir.~~ It is
434 generally known that glaciers facing the north are more developed in HMA. Due to the orientation of the mountains, most of
435 the large glaciers ~~in Karakoram and Pamir~~ flow toward the north and northeast. ~~The~~ Besides, the area-to-number ratio of
436 largesurging glaciers ~~flowing towards the northwest~~ is much ~~less~~ larger than non-surging glaciers in the northeast orientation,
437 but smaller in the northwest orientation. This is true for the Karakoram, Pamirs, and West Kunlun Shan, the three largest
438 clusters of surging glaciers, indicates that large northeast-facing glacier has higher possibility to be surging glacier.
439 Accordingly, the surging glaciers facing the north and northeast ~~are much more~~ have higher area ratio than that facing the
440 northwest ~~(see Fig. 5). The number of surging glaciers in Karakoram and Pamir accounts for a considerable proportion of the~~
441 ~~total number of surging glaciers in HMA, and therefore the orientation of surging glaciers there has a great impact on the~~
442 ~~orientation distribution of surging glaciers in HMA.~~

443 The spatial distribution of surging glaciers in HMA presents strong heterogeneity. About 83% of identified surging glaciers
444 were located in the northwest region including the Central Tien Shan, Pamirs, Karakoram, and West Kunlun, and their area
445 occupied about 87% of the total identified surging glacier area (see Fig. 4 and Table 2). As discussed above, larger glaciers

446 are more likely to surge. The northwest regions generally hold more large glaciers, and therefore hold more surging glaciers.
447 In other subregions, large glaciers are usually concentrated in some great ice fields, such as the Geladandong, Puruogangri,
448 and Xinqingfeng. Accordingly, surging glaciers in these subregions are usually clustered in several watersheds.
449 Several studies have pointed out that glacier surge activities have little impact on the glacier mass balance (Gardelle et al.,
450 2013; Bolch et al., 2017; Guillet et al., 2022). However, glacier mass balance may also affect the occurrence of glacier surge.
451 Copland et al. (2011) concluded that the increase of glacier surges in the Karakoram could be related to the positive mass
452 budget. The accumulated ice mass would accelerate a glacier to surge (Eisen et al., 2005; Kochtitzky et al., 2020), and the
453 significant mass loss could prevent or postpone the surge in return (Dowdeswell et al., 1995). On a regional large scale, the
454 relationship between mass balance and surge occurrence needs to be further analysed. Our glacier elevation change maps of
455 the period 2000-2010s are similar to that derived by Brun et al. (2017) and Shean et al. (2020). We found that, at the regional
456 scale, the occurrence of surging glaciers is correlated with the regional glacier mass balance. The three subregions holding the
457 largest clusters of surging glaciers, i.e., the Pamirs, Karakoram, and West Kunlun, are characterized by slightly negative or
458 positive mass budgets, which is known as the ‘Pamir-Karakoram-West Kunlun’ anomaly (Brun et al., 2017). Likewise, the
459 subregions Central Tien Shan, Tibetan Interior Mountains, and East Kunlun Shan, which hold the moderate clusters of surging
460 glaciers, have glacier mass loss rates much lower than the average rates of HMA. By contrast, subregions with severe glacier
461 mass loss hold the lowest surging glacier ratio, such as the Dzhungarsky Alatau, Hengduan Shan, and Eastern Himalaya.

462 **6.3 Comparison with previous surging glacier inventories**

463 Guillet et al. (2022) presented a comprehensive surging glacier inventory of HMA for the period 2000-2018 from a multi-
464 factor remote sensing approach. Prior to the comparison, we generated an inventory based on the RGI6.0, as Guillet et al.
465 (2022) did. Guillet et al. (2022) identified 666 surging glaciers, and the area of surging glacier occupies 19.5% of the total
466 glacier area. We identified 890 surging glaciers (809 if RGI6.0 was used), and their area only occupies 16.59% of the total
467 glacier area. We attributed the lower area ratio of surging glaciers to two reasons. First, in our inventory the surging tributaries
468 were separated from the non-surging trunks. Second, many outcrop rocks and shaded areas are excluded from the GAMDAM2
469 glacier areas (Sakai, 2019), which would lower our surging area ratio, but make the result more accurate. If we assign our
470 identified surging glaciers to the RGI6.0 polygons without tributary separation, the surging area ratio would be larger (20.25%).
471 Within our inventory, 556 surging and 62 surge-like glaciers were also identified by Guillet et al. (2022), and the discrepancy
472 of identifications mostly occurred on small glaciers. If only the period 2000-2020 was considered, 657 surging glaciers were
473 identified by us, which is very close to that of Guillet et al. (665). For the period 1970s-2000, there are 151 surging and 101
474 surge-like glaciers that were not identified by Guillet et al. (2022). Overall, we have newly identified 253 surging and 248
475 surge-like glaciers. We owed the newly findings to the longer observation period and multiple elevation change observation.
476 However, 47 surging glacier presented by Guillet et al. were missed in this study, and 62 surge-like glaciers in our new
477 inventory were identified as surging glaciers by Guillet et al. (2022). We carefully checked the glaciers not included in our
478 inventory but included in Guillet et al.’s inventory, as well as those included in our inventory but not included in Guillet et al.’s
479 inventory, and this step helped us to find 21 more surging glaciers. We attribute this to the deficiency of using a single criterion,
480 which could be aided by combining other features. Besides, the DEMs used in this study were suffering from the data voids
481 and incomplete spatial coverage, especially for the KH-9 DEM, which could result in a relatively conservative identification.
482 Multiple studies have identified surging glaciers in the Karakoram based on different data sources. For example, Bhambri et
483 al. (2017) identified 221 surging and surge-like glaciers (the tributaries of a glacier system are counted as individual glaciers)
484 based on the glacier morphology changes detected from spaceborne optical images acquired from 1972 to 2016, in-situ
485 observations, and archive photos since the 1840s. However, the boundary used by Bhambri et al. (2017) to define the extent
486 of Karakoram is much smaller than that used in our inventory. A much smaller group of surging glaciers (88) were identified
487 by Copland et al. (2011) based on a similar method and the data acquired between 1960 and 2013. Rankl et al. (2014) identified

488 101 surging glaciers in the Karakoram by detecting the changes in glacier surface velocity and terminus position between 1976
489 and 2012. The results of Guillet et al. (2022) should be more reliable than previous ones, because more criteria were used for
490 identifying surging glaciers. Compared with previous inventories, our inventory includes more surging glaciers (354). Among
491 the 223 surging glaciers in the Karakoram identified by Guillet et al. (2022), 203 were identified as surging glaciers, and 12
492 were identified as surge-like glaciers in this study, which means only 8 surging glaciers presented by Guillet et al. (2022) were
493 not included in our inventory. The high coincidence between the two inventories indicates our surging glacier identification
494 result is reliable. In total, we have newly identified 101 surging and 101 surge-like glaciers in this region.

495 Based on the method of glacier terminus change monitoring in Google Earth Engine, Vale et al. (2021) identified obvious
496 terminus change of 137 surging glaciers. We found 127 verified surging and 6 surge-like glaciers in our inventory were
497 included in their inventory, i.e., only four glaciers were missed in this study. The possible reason for this gap is that the
498 technique used by Vale et al. cannot identify the internal glacier surges than did not cause terminus advancing. Also, the
499 inadequate quality and spatial resolution of satellite images could limit the performance of detecting changes in glacier
500 terminus position.

501 In the Pamirs, Sevestre and Been (2015) identified 820 surge-type glaciers based on publications and reports, but Goerlich et
502 al. (2020) reported only 186 surging glaciers based on the observations of glacier flow velocity, elevation change, etc.. We
503 found that, if Goerlich et al. (2020) applied the GAMDAM2 glacier polygons used in this study, the number of identified
504 surging glaciers should be 182. Among the 182 surging glaciers identified by Goerlich et al. (2020), 153 and 15 were identified
505 as surging and surge-like glaciers in our study, respectively. Although 14 surging glaciers are missed in this study, our
506 inventory has contained other 94 surging and 44 surge-like glaciers. The main cause for the result discrepancy is that the glacier
507 elevation change observation conducted by Goerlich et al. (2020) only covered parts of the Western Pamir and only the
508 observations before 2000 were used. In this region our inventory shared 193 surging glaciers with Guillet et al's inventory,
509 and 185 of them were identified during the period 2000-2020, which also manifests a high coincidence of the two results.

510 In the West Kunlun, Yasuda and Furuya (2015) reported 9 surging glaciers in the main range only, based on changes in glacier
511 flow velocity and terminus position of 31 glaciers, and other 9 surging glaciers were found in the northwest part of the West
512 Kunlun Shan by Chudley et al. (2019). A larger number (60) were found by Guillet et al. (2022). However, our inventory has
513 even included more surging (82) and surge-like (47) glaciers in the West Kunlun Shan. During the period 2000-2020, we have
514 identified 61 surging glaciers, which is very close to the number presented by Guillet et al. (2022). In Central Tien Shan,
515 Mukherjee et al. (2017) identified 39 surge-type (including 9 surging and 30 surge-like 13 very probable surging) glaciers
516 through the analysis of changes in surface elevation and morphology from 1964 to 2014, whereas 79 (59 surging and 20 surge-
517 like) were identified in our studies. The insufficient coverage of elevation change observation (only covered the west part of
518 the Central Tien Shan) may be the main reason for the discrepancy in identification results. Guillet et al. (2022) identified 54
519 surging glaciers during 2000-2018, in which 36 were confirmed in our inventory.

520 7 Conclusions

521 This study presented a new inventory of surging glaciers across the entire HMA range, which was accomplished based on the
522 glacier surface elevation changes derived from multiple elevation sources, by using the morphological ~~feature~~ changes from
523 optical images as complements. In total 890 surging and 336 surge-like glaciers were identified in the new inventory. Through
524 the analysis of geometric parameters, we found that surging glaciers generally have a greater area, length, and elevation range
525 than non-surging glaciers. However, the differences are smaller ~~than we thought~~ if taking the glacier size distribution into
526 account. When considering glaciers having of similar area, the steeper ~~one is ones are~~ more likely to surge. Furthermore,
527 ~~combining~~ combining the region-wide glacier mass balance measurements, we found a similar distribution between the positive
528 mass balance and number of surging glaciers. Benefiting from the long period and wide coverage of surface elevation change

529 observations, our study ~~newly~~ identified ~~much more~~ 253 surging and 248 surge-like glaciers in HMA than in previous ~~inventory~~
530 (Guillet et al., 2022) ~~studies~~. However, our inventory does not provide the surge duration period and the maximum flow
531 velocity to describe the dynamic process of each glacier surge activity. Improvements should be made by combining multi-
532 criteria identification methods. Considering the fact that glacier surges are more widespread than we thought, the inventory
533 presented in this study still needs further replenishment.

534 **8 Data and code availability**

535 The presented inventory ~~and corresponding multi-temporal elevation change results of identified surging glaciers is~~ are freely
536 available at: <https://doi.org/10.5281/zenodo.7590838> (Guo et al., 2022). ~~The dataset is composed of two files including the~~
537 ~~inventory itself and the associated metadata file~~. The inventory is distributed in the format of GeoPackage (.gpkg) and ESRI
538 shpfile (.shp), which is represented by outline or ~~centroid~~ manually defined center point of surging glaciers with geometric
539 attributes. The glacier polygons of the inventory are compiled from the GAMDAM2 glacier inventory. In total eight fields are
540 integrated in the attributes table to describe the surging information of corresponding glacier as mentioned in section 4.3. The
541 description of each field in the attribute table is listed in Table 3. ~~The DEM differencing results of COP30 DEM - NASADEM,~~
542 ~~HMA8m DEM - NASADEM, and NASADEM - KH-9 DEM are compressed into individual zip file, respectively. The~~
543 ~~elevation change results of surging glaciers were divided into multi-temporal 1° × 1° tiled GeoTiff grids~~. The metadata file is
544 stored in a text file (README.txt), which contains the ~~datasets~~ description and details of the attributes information of the
545 inventory.

546 The code used for elevation change estimation can be available at: https://github.com/TristanBlus/dem_coreg. This code was
547 developed based on the *demcoreg* package (Shean et al., 2019).

548 **Author contribution**

549 J.L. and L.G. conceived this study and wrote the paper. L.G. developed the processing flow, compiled the inventory and drew
550 the figures with the support from J.L. A.D. generated the KH-9 DEM. A.D., Z.L. and X.L. helped with the results analysis and
551 discussions and manuscript editing. Z.L., J.L. and J.Z. provided the funding acquisition. All authors have contributed and
552 agreed to the published version of the manuscript.

553 **Competing interest**

554 The authors declare that they have no conflict of interest.

555 **Acknowledgments**

556 The authors express gratitude to all institution that provide us the opensource dataset used in this study: the NASADEM from
557 LP DAAC (https://e4ftl01.cr.usgs.gov/MEASURES/NASADEM_HGT.001/), the Copernicus DEM from European Space
558 Agency (ESA) (<https://spacedata.copernicus.eu/web/cscda/cop-dem-faq>), the HMA8m DEM processed by David Shean from
559 National Snow and Ice Data Center (NSIDC) (https://nsidc.org/data/HMA_DEM8m_MOS/versions/1), and the Randolph
560 Glacier Inventory Version 6.0 (<http://www.glims.org/RGI/randolph.html>). The authors also appreciate the valuable comments
561 from Frank Pual and Guillet Gregoire.

562 **Financial support**

563 This work was supported by the National Natural Science Fund for Distinguished Young Scholars (41925016), the Strategic
564 Priority Research Program of Chinese Academy of Sciences (XDA20100101), the National Natural Science Foundation of
565 China (41904006), the Hunan Key Laboratory of remote sensing of ecological environment in Dongting Lake Area (No. 2021-
566 010), the Fundamental Research Funds for the Central Universities of Central South University (2021zzts0265).

567 **References**

- 568 Abdel Jaber, W., Rott, H., Floricioiu, D., Wuite, J., and Miranda, N.: Heterogeneous spatial and temporal pattern of surface
569 elevation change and mass balance of the Patagonian ice fields between 2000 and 2016, *The Cryosphere*, 13, 2511–2535,
570 doi:10.5194/tc-13-2511-2019, 2019.
- 571 AIRBUS: Copernicus Digital Elevation Model Validation Report, AIRBUS Defence and Space GmbH, 2020.
- 572 An, B., Wang, W., Yang, W., Wu, G., Guo, Y., Zhu, H., Gao, Y., Bai, L., Zhang, F., Zeng, C., Wang, L., Zhou, J., Li, X., Li,
573 J., Zhao, Z., Chen, Y., Liu, J., Li, J., Wang, Z., Chen, W., and Yao, T.: Process, mechanisms, and early warning of glacier
574 collapse-induced river blocking disasters in the Yarlung Tsangpo Grand Canyon, southeastern Tibetan Plateau, *Sci. Total*
575 *Environ.*, 151652, doi:10.1016/j.scitotenv.2021.151652, 2021.
- 576 Barrand, N. E. and Murray, T.: Multivariate Controls on the Incidence of Glacier Surging in the Karakoram Himalaya, *Arct.*
577 *Antarct. Alp. Res.*, 38, 489–498, doi:10.1657/1523-0430(2006)38[489:MCOTIO]2.0.CO;2, 2006.
- 578 Beaud, F., Aati, S., Delaney, I., Adhikari, S., and Avouac, J.-P.: Generalized sliding law applied to the surge dynamics of
579 Shisper Glacier and constrained by timeseries correlation of optical satellite images, *Glaciers/Remote Sensing*, doi:10.5194/tc-
580 2021-96, 2021.
- 581 Benn, D. I., Fowler, A. C., Hewitt, I., and Sevestre, H.: A general theory of glacier surges, *J. Glaciol.*, 65, 701–716,
582 doi:10.1017/jog.2019.62, 2019.
- 583 Bhambri, R., Hewitt, K., Kawishwar, P., and Pratap, B.: Surge-type and surge-modified glaciers in the Karakoram, *Sci. Rep.*,
584 7, doi:10.1038/s41598-017-15473-8, 2017.
- 585 Bhambri, R., Hewitt, K., Haritashya, U. K., Chand, P., Kumar, A., Verma, A., Tiwari, S. K., and Rai, S. K.: Characteristics of
586 surge-type tributary glaciers, Karakoram, *Geomorphology*, 403, 108161, doi:10.1016/j.geomorph.2022.108161, 2022.
- 587 Bolch, T., Kulkarni, A., Kaab, A., Huggel, C., Paul, F., Cogley, J. G., Frey, H., Kargel, J. S., Fujita, K., Scheel, M., Bajracharya,
588 S., and Stoffel, M.: The State and Fate of Himalayan Glaciers, *Science*, 336, 310–314, doi:10.1126/science.1215828, 2012.
- 589 Bolch, T., Pieczonka, T., Mukherjee, K., and Shea, J.: Brief communication: Glaciers in the Hunza catchment (Karakoram)
590 have been nearly in balance since the 1970s, *The Cryosphere*, 11, 531–539, doi:10.5194/tc-11-531-2017, 2017.
- 591 Bolch, T., Shea, J. M., Liu, S., Azam, F. M., Gao, Y., Gruber, S., Immerzeel, W. W., Kulkarni, A., Li, H., Tahir, A. A., Zhang,
592 G., and Zhang, Y.: Status and Change of the Cryosphere in the Extended Hindu Kush Himalaya Region, in: *The Hindu Kush*
593 *Himalaya Assessment*, edited by: Wester, P., Mishra, A., Mukherji, A., and Shrestha, A. B., Springer International Publishing,
594 Cham, 209–255, doi:10.1007/978-3-319-92288-1_7, 2019.
- 595 Brun, F., Berthier, E., Wagnon, P., Käab, A., and Treichler, D.: A spatially resolved estimate of High Mountain Asia glacier
596 mass balances from 2000 to 2016, *Nat. Geosci.*, 10, 668–673, doi:10.1038/ngeo2999, 2017.
- 597 Chudley, T. R. and Willis, I. C.: Glacier surges in the north-west West Kunlun Shan inferred from 1972 to 2017 Landsat
598 imagery, *J. Glaciol.*, 65, 1–12, doi:10.1017/jog.2018.94, 2019.
- 599 Clarke, G. K. C.: Length, width and slope influences on glacier surging, *J. Glaciol.*, 37, 236–246,
600 doi:10.3189/S0022143000007255, 1991.
- 601 Clarke, G. K. C., Schmok, J. P., Ommanney, C. S. L., and Collins, S. G.: Characteristics of surge-type glaciers, *J. Geophys.*
602 *Res. Solid Earth*, 91, 7165–7180, doi:10.1029/JB091iB07p07165, 1986.

603 Cogley, J. G., Arendt, A. A., Bauder, A., Braithwaite, R. J., Hock, R., J, B., R., Jansson, P., Kaser, G., Moller, M., Nicholson,
604 L., Rasmussen, L. A., and Zemp, M.: Glossary of glacier mass balance and related terms, IACS Contribution No.2, UNESCO,
605 Paris, 2011.

606 Copland, L., Sylvestre, T., Bishop, M. P., Shroder, J. F., Seong, Y. B., Owen, L. A., Bush, A., and Kamp, U.: Expanded and
607 Recently Increased Glacier Surging in the Karakoram, *Arct. Antarct. Alp. Res.*, 43, 503–516, 2011.

608 Crippen, R., Buckley, S., Agram, P., Belz, E., Gurrola, E., Hensley, S., Kobrick, M., Lavallo, M., Martin, J., Neumann, M.,
609 Nguyen, Q., Rosen, P., Shimada, J., Simard, M., and Tung, W.: NASADEM global elevation model: methods and progress,
610 *ISPRS - Int. Arch. Photogramm. Remote Sens. Spat. Inf. Sci.*, XLI-B4, 125–128, doi:10.5194/isprsarchives-XLI-B4-125-2016,
611 2016.

612 Dehecq, A., Gardner, A. S., Alexandrov, O., McMichael, S., Hugonnet, R., Shean, D., and Marty, M.: Automated Processing
613 of Declassified KH-9 Hexagon Satellite Images for Global Elevation Change Analysis Since the 1970s, *Front. Earth Sci.*, 8,
614 566802, doi:10.3389/feart.2020.566802, 2020.

615 Dowdeswell, J. A., Hodgkins, R., Nuttall, A.-M., Hagen, J. O., and Hamilton, G. S.: Mass balance change as a control on the
616 frequency and occurrence of glacier surges in Svalbard, Norwegian High Arctic, *Geophys. Res. Lett.*, 22, 2909–2912,
617 doi:10.1029/95GL02821, 1995.

618 Eisen, O., Harrison, W. D., Raymond, C. F., Echelmeyer, K. A., Bender, G. A., and Gorda, J. L. D.: Variegated Glacier, Alaska,
619 USA: a century of surges, *J. Glaciol.*, 51, 399–406, doi:10.3189/172756505781829250, 2005.

620 Fan, Y., Ke, C.-Q., Zhou, X., Shen, X., Yu, X., and Lhakpa, D.: Glacier mass-balance estimates over High Mountain Asia
621 from 2000 to 2021 based on ICESat-2 and NASADEM, *J. Glaciol.*, 1–13, doi:10.1017/jog.2022.78, 2022.

622 Farinotti, D., Immerzeel, W. W., Kok, R., Quincey, D. J., and Dehecq, A.: Manifestations and mechanisms of the Karakoram
623 glacier Anomaly, *Nat. Geosci.*, 13, 8–16, doi:10.1038/s41561-019-0513-5, 2020.

624 Farnsworth, W. R., Ingólfsson, Ó., Retelle, M., and Schomacker, A.: Over 400 previously undocumented Svalbard surge-type
625 glaciers identified, *Geomorphology*, 264, 52–60, doi:10.1016/j.geomorph.2016.03.025, 2016.

626 Farr, T. G., Rosen, P. A., Caro, E., Crippen, R., Duren, R., Hensley, S., Kobrick, M., Paller, M., Rodriguez, E., Roth, L., Seal,
627 D., Shaffer, S., Shimada, J., Umland, J., Werner, M., Oskin, M., Burbank, D., and Alsdorf, D.: The Shuttle Radar Topography
628 Mission, *Rev. Geophys.*, 45, RG2004, doi:10.1029/2005RG000183, 2007.

629 Fowler, A. C.: A theory of glacier surges, *J. Geophys. Res.*, 92, 9111, doi:10.1029/JB092iB09p09111, 1987.

630 Fowler, A. C., Murray, T., and Ng, F. S. L.: Thermally controlled glacier surging, *J. Glaciol.*, 47, 527–538,
631 doi:10.3189/172756501781831792, 2001.

632 Gardelle, J., Berthier, E., Arnaud, Y., and Käab, A.: Region-wide glacier mass balances over the Pamir-Karakoram-Himalaya
633 during 1999–2011, *Cryosphere Discuss.*, 7, 975–1028, doi:10.5194/tcd-7-975-2013, 2013.

634 Goerlich, F., Bolch, T., and Paul, F.: More dynamic than expected: an updated survey of surging glaciers in the Pamir, *Earth
635 Syst. Sci. Data*, 12, 3161–3176, doi:10.5194/essd-12-3161-2020, 2020.

636 Guillet, G., King, O., Lv, M., Ghuffar, S., Benn, D., Quincey, D., and Bolch, T.: A regionally resolved inventory of High
637 Mountain Asia surge-type glaciers, derived from a multi-factor remote sensing approach, *The Cryosphere*, 16, 603–623,
638 doi:10.5194/tc-16-603-2022, 2022.

639 Guth, P. L. and Geoffroy, T. M.: LiDAR point cloud and ICESat-2 evaluation of 1 second global digital elevation models:
640 Copernicus wins, *Trans. GIS*, 25, 2245–2261, doi:10.1111/tgis.12825, 2021.

641 Hewitt, K.: The Karakoram Anomaly? Glacier Expansion and the ‘Elevation Effect,’ *Karakoram Himalaya, Mt. Res. Dev.*, 25,
642 332–340, doi:10.1659/0276-4741(2005)025[0332:TKAGEA]2.0.CO;2, 2005.

643 Hewitt, K.: Tributary glacier surges: an exceptional concentration at Panmah Glacier, Karakoram Himalaya, *J. Glaciol.*, 53,
644 181–188, doi:10.3189/172756507782202829, 2007.

645 Höhle, J. and Höhle, M.: Accuracy assessment of digital elevation models by means of robust statistical methods, *ISPRS J.*
646 *Photogramm. Remote Sens.*, 64, 398–406, doi:10.1016/j.isprsjprs.2009.02.003, 2009.

647 Holzer, N., Vijay, S., Yao, T., Xu, B., Buchroithner, M., and Bolch, T.: Four decades of glacier variations at Muztagh Ata
648 (eastern Pamir): a multi-sensor study including Hexagon KH-9 and Pléiades data, *The Cryosphere*, 9, 2071–2088,
649 doi:10.5194/tc-9-2071-2015, 2015.

650 Hugonnet, R., McNabb, R., Berthier, E., Menounos, B., Nuth, C., Girod, L., Farinotti, D., Huss, M., Dussailant, I., Brun, F.,
651 and Kääb, A.: Accelerated global glacier mass loss in the early twenty-first century, *Nature*, 592, 726–731,
652 doi:10.1038/s41586-021-03436-z, 2021.

653 Jacquemart, M. and Cicoira, A.: Hazardous Glacier Instabilities: Ice Avalanches, Sudden Large-Volume Detachments of Low-
654 Angle Mountain Glaciers, and Glacier Surges, in: *Treatise on Geomorphology*, Elsevier, 330–345, doi:10.1016/B978-0-12-
655 818234-5.00188-7, 2022.

656 Jiskoot, H.: Glacier Surging, in: *Encyclopedia of Snow, Ice and Glaciers*, edited by: Singh, V. P., Singh, P., and Haritashya,
657 U. K., Springer Netherlands, Dordrecht, 415–428, doi:10.1007/978-90-481-2642-2_559, 2011.

658 Jiskoot, H., Murray, T., and Boyle, P.: Controls on the distribution of surge-type glaciers in Svalbard, *J. Glaciol.*, 46, 412–422,
659 doi:10.3189/172756500781833115, 2000.

660 Kääb, A., Leinss, S., Gilbert, A., Bühler, Y., Gascoïn, S., Evans, S. G., Bartelt, P., Berthier, E., Brun, F., Chao, W.-A., Farinotti,
661 D., Gimbert, F., Guo, W., Huggel, C., Kargel, J. S., Leonard, G. J., Tian, L., Treichler, D., and Yao, T.: Massive collapse of
662 two glaciers in western Tibet in 2016 after surge-like instability, *Nat. Geosci.*, 11, 114–120, doi:10.1038/s41561-017-0039-7,
663 2018.

664 Kääb, A., Jacquemart, M., Gilbert, A., Leinss, S., Girod, L., Huggel, C., Falaschi, D., Ugalde, F., Petrakov, D., Chernomorets,
665 S., Dokukin, M., Paul, F., Gascoïn, S., Berthier, E., and Kargel, J. S.: Sudden large-volume detachments of low-angle mountain
666 glaciers – more frequent than thought?, *The Cryosphere*, 15, 1751–1785, doi:10.5194/tc-15-1751-2021, 2021.

667 Kamb, B.: Glacier surge mechanism based on linked cavity configuration of the basal water conduit system, *J. Geophys. Res.*,
668 92, 9083, doi:10.1029/JB092iB09p09083, 1987.

669 Kochtitzky, W., Winski, D., McConnell, E., Kreutz, K., Campbell, S., Enderlin, E. M., Copland, L., Williamson, S., Main, B.,
670 and Jiskoot, H.: Climate and surging of Donjek Glacier, Yukon, Canada, *Arct. Antarct. Alp. Res.*, 52, 264–280,
671 doi:10.1080/15230430.2020.1744397, 2020.

672 Li, J., Li, Z., Zhu, J., Li, X., Xu, B., Wang, Q., Huang, C., and Hu, J.: Early 21st century glacier thickness changes in the
673 Central Tien Shan, *Remote Sens. Environ.*, 192, 12–29, doi:10.1016/j.rse.2017.02.003, 2017.

674 Lv, M., Guo, H., Lu, X., Liu, G., Yan, S., Ruan, Z., Ding, Y., and Quincey, D. J.: Characterizing the behaviour of surge- and
675 non-surge-type glaciers in the Kingata Mountains, eastern Pamir, from 1999 to 2016, *The Cryosphere*, 13, 219–236,
676 doi:10.5194/tc-13-219-2019, 2019.

677 Lv, M., Guo, H., Yan, J., Wu, K., Liu, G., Lu, X., Ruan, Z., and Yan, S.: Distinguishing Glaciers between Surging and
678 Advancing by Remote Sensing: A Case Study in the Eastern Karakoram, *Remote Sens.*, 12, 2297, doi:10.3390/rs12142297,
679 2020.

680 Maurer, J. M., Schaefer, J. M., Rupper, S., and Corley, A.: Acceleration of ice loss across the Himalayas over the past 40 years,
681 *Sci. Adv.*, 5, eaav7266, doi:10.1126/sciadv.aav7266, 2019.

682 Maussion, F., Scherer, D., Mölg, T., Collier, E., Curio, J., and Finkelnburg, R.: Precipitation Seasonality and Variability over
683 the Tibetan Plateau as Resolved by the High Asia Reanalysis, *J. Clim.*, 27, 1910–1927, doi:10.1175/JCLI-D-13-00282.1, 2014.

684 Maussion, F., Butenko, A., Champollion, N., Dusch, M., Eis, J., Fourteau, K., Gregor, P., Jarosch, A. H., Landmann, J.,
685 Oesterle, F., Recinos, B., Rothenpieler, T., Vlug, A., Wild, C. T., and Marzeion, B.: The Open Global Glacier Model (OGGM)
686 v1.1, *Geosci. Model Dev.*, 12, 909–931, doi:10.5194/gmd-12-909-2019, 2019.

687 Muhammad, S., Li, J., Steiner, J. F., Shrestha, F., Shah, G. M., Berthier, E., Guo, L., Wu, L., and Tian, L.: A holistic view of
688 Shisper Glacier surge and outburst floods: from physical processes to downstream impacts, *Geomat. Nat. Hazards Risk*, 12,
689 2755–2775, doi:10.1080/19475705.2021.1975833, 2021.

690 Mukherjee, K., Bolch, T., Goerlich, F., Kutuzov, S., Osmonov, A., Pieczonka, T., and Shesterova, I.: Surge-Type Glaciers in
691 the Tien Shan (Central Asia), *Arct. Antarct. Alp. Res.*, 49, 147–171, doi:10.1657/AAAR0016-021, 2017.

692 Murray, T., Strozzi, T., Luckman, A., Jiskoot, H., and Christakos, P.: Is there a single surge mechanism? Contrasts in dynamics
693 between glacier surges in Svalbard and other regions: IS THERE A SINGLE SURGE MECHANISM?, *J. Geophys. Res. Solid*
694 *Earth*, 108, doi:10.1029/2002JB001906, 2003.

695 Nuimura, T., Sakai, A., Taniguchi, K., Nagai, H., Lamsal, D., Tsutaki, S., Kozawa, A., Hoshina, Y., Takenaka, S., Omiya, S.,
696 Tsunematsu, K., Tshering, P., and Fujita, K.: The GAMDAM glacier inventory: a quality-controlled inventory of Asian
697 glaciers, *The Cryosphere*, 9, 849–864, doi:10.5194/tc-9-849-2015, 2015.

698 Nuth, C. and Kääb, A.: Co-registration and bias corrections of satellite elevation data sets for quantifying glacier thickness
699 change, *The Cryosphere*, 5, 271–290, doi:10.5194/tc-5-271-2011, 2011.

700 Paul, F.: Revealing glacier flow and surge dynamics from animated satellite image sequences: examples from the Karakoram,
701 *The Cryosphere*, 9, 2201–2214, doi:10.5194/tc-9-2201-2015, 2015.

702 Paul, F.: Repeat Glacier Collapses and Surges in the Amney Machen Mountain Range, Tibet, Possibly Triggered by a
703 Developing Rock-Slope Instability, *Remote Sens.*, 11, 708, doi:10.3390/rs11060708, 2019.

704 Purinton, B. and Bookhagen, B.: Beyond Vertical Point Accuracy: Assessing Inter-pixel Consistency in 30 m Global DEMs
705 for the Arid Central Andes, *Front. Earth Sci.*, 9, 758606, doi:10.3389/feart.2021.758606, 2021.

706 Quincey, D. J., Braun, M., Glasser, N. F., Bishop, M. P., Hewitt, K., and Luckman, A.: Karakoram glacier surge dynamics,
707 *Geophys. Res. Lett.*, 38, n/a-n/a, doi:10.1029/2011GL049004, 2011.

708 Rankl, M., Kienholz, C., and Braun, M.: Glacier changes in the Karakoram region mapped by multitemporal satellite imagery,
709 *The Cryosphere*, 8, 977–989, doi:10.5194/tc-8-977-2014, 2014.

710 Round, V., Leinss, S., Huss, M., Haemmig, C., and Hajnsek, I.: Surge dynamics and lake outbursts of Kyagar Glacier,
711 Karakoram, *The Cryosphere*, 11, 723–739, doi:10.5194/tc-11-723-2017, 2017.

712 Sakai, A.: Brief communication: Updated GAMDAM glacier inventory over high-mountain Asia, *The Cryosphere*, 13, 2043–
713 2049, doi:10.5194/tc-13-2043-2019, 2019.

714 Sevestre, H. and Benn, D. I.: Climatic and geometric controls on the global distribution of surge-type glaciers: implications
715 for a unifying model of surging, *J. Glaciol.*, 61, 646–662, doi:10.3189/2015JoG14J136, 2015.

716 Shean, D., Shashank Bhushan, Lilien, D., and Meyer, J.: dshean/demcoreg: Zenodo DOI release, ,
717 doi:10.5281/ZENODO.3243481, 2019.

718 Shean, D. E., Alexandrov, O., Moratto, Z. M., Smith, B. E., Joughin, I. R., Porter, C., and Morin, P.: An automated, open-
719 source pipeline for mass production of digital elevation models (DEMs) from very-high-resolution commercial stereo satellite
720 imagery, *ISPRS J. Photogramm. Remote Sens.*, 116, 101–117, doi:10.1016/j.isprsjprs.2016.03.012, 2016.

721 Shean, D. E., Bhushan, S., Montesano, P., Rounce, D. R., Arendt, A., and Osmanoglu, B.: A Systematic, Regional Assessment
722 of High Mountain Asia Glacier Mass Balance, *Front. Earth Sci.*, 7, 363, doi:10.3389/feart.2019.00363, 2020.

723 Shugar, D. H., Jacquemart, M., Shean, D., Bhushan, S., Upadhyay, K., Sattar, A., Schwanghart, W., McBride, S., de Vries, M.,
724 V. W., Mergili, M., Emmer, A., Deschamps-Berger, C., McDonnell, M., Bhambri, R., Allen, S., Berthier, E., Carrivick, J. L.,
725 Clague, J. J., Dokukin, M., Dunning, S. A., Frey, H., Gascoïn, S., Haritashya, U. K., Huggel, C., Kääb, A., Kargel, J. S.,
726 Kavanaugh, J. L., Lacroix, P., Petley, D., Rupper, S., Azam, M. F., Cook, S. J., Dimri, A. P., Eriksson, M., Farinotti, D., Fiddes,
727 J., Gnyawali, K. R., Harrison, S., Jha, M., Koppes, M., Kumar, A., Leinss, S., Majeed, U., Mal, S., Muhuri, A., Noetzli, J.,
728 Paul, F., Rashid, I., Sain, K., Steiner, J., Ugalde, F., Watson, C. S., and Westoby, M. J.: A massive rock and ice avalanche
729 caused the 2021 disaster at Chamoli, Indian Himalaya, *Science*, 373, 300–306, doi:10.1126/science.abh4455, 2021.

- 730 Steiner, J. F., Kraaijenbrink, P. D. A., Jiduc, S. G., and Immerzeel, W. W.: Brief communication: The Khurdopin glacier surge
 731 revisited – extreme flow velocities and formation of a dammed lake in 2017, *The Cryosphere*, 12, 95–101, doi:10.5194/tc-12-
 732 95-2018, 2018.
- 733 Surazakov, A. and Aizen, V.: Positional Accuracy Evaluation of Declassified Hexagon KH-9 Mapping Camera Imagery,
 734 *Photogramm. Eng. Remote Sens.*, 76, 603–608, doi:10.14358/PERS.76.5.603, 2010.
- 735 Thøgersen, K., Gilbert, A., Schuler, T. V., and Malthe-Sørenssen, A.: Rate-and-state friction explains glacier surge propagation,
 736 *Nat. Commun.*, 10, 2823, doi:10.1038/s41467-019-10506-4, 2019.
- 737 Vale, A. B., Arnold, N. S., Rees, W. G., and Lea, J. M.: Remote Detection of Surge-Related Glacier Terminus Change across
 738 High Mountain Asia, *Remote Sens.*, 13, 1309, doi:10.3390/rs13071309, 2021.
- 739 Van Wyk de Vries, M., Wickert, A. D., MacGregor, K. R., Rada, C., and Willis, M. J.: Atypical landslide induces speedup,
 740 advance, and long-term slowdown of a tidewater glacier, *Geology*, doi:10.1130/G49854.1, 2022.
- 741 Yamazaki, D., Ikeshima, D., Tawatari, R., Yamaguchi, T., O’Loughlin, F., Neal, J. C., Sampson, C. C., Kanae, S., and Bates,
 742 P. D.: A high-accuracy map of global terrain elevations, *Geophys. Res. Lett.*, 44, 5844–5853, doi:10.1002/2017GL072874,
 743 2017.
- 744 Yasuda, T. and Furuya, M.: Dynamics of surge-type glaciers in West Kunlun Shan, Northwestern Tibet: SURGE-TYPE
 745 GLACIERS IN WEST KUNLUN SHAN, *J. Geophys. Res. Earth Surf.*, 120, 2393–2405, doi:10.1002/2015JF003511, 2015.
- 746 Zhou, S., Yao, X., Zhang, D., Zhang, Y., Liu, S., and Min, Y.: Remote Sensing Monitoring of Advancing and Surging Glaciers
 747 in the Tien Shan, 1990–2019, *Remote Sens.*, 13, 1973, doi:10.3390/rs13101973, 2021.
- 748 Zhou, Y., Li, Z., and Li, J.: Slight glacier mass loss in the Karakoram region during the 1970s to 2000 revealed by KH-9
 749 images and SRTM DEM, *J. Glaciol.*, 63, 331–342, doi:10.1017/jog.2016.142, 2017.
- 750 Zhou, Y., Li, Z., Li, J., Zhao, R., and Ding, X.: Glacier mass balance in the Qinghai–Tibet Plateau and its surroundings from
 751 the mid-1970s to 2000 based on Hexagon KH-9 and SRTM DEMs, *Remote Sens. Environ.*, 210, 96–112,
 752 doi:10.1016/j.rse.2018.03.020, 2018.

753 Tables and Figures

754 **Table 1: Surging glacier identification results**

| Glacier changes | Identification class | | | Total |
|--|----------------------|----------------|----------------|-------|
| | I | II | III | |
| 2000-2020 elevation change | 719 | 157 | 169 | 1045 |
| 1970s-2000 elevation change | 507 | 156 | 57 | 720 |
| 1986-2021 terminus advance | 247 | 397 | - | 645 |
| 1986-2021 looped moraine | 112 | 31 | - | 144 |
| 1986-2021 medial moraine | 69 | 29 | - | 108 |
| Final identified surging glaciers | 890 (verified) | 208 (probable) | 128 (possible) | 1226 |

755 **Table 2: Results of surging glacier identification in 22 subregions of HMA. Only glaciers larger than 0.4 km² were considered in the**
 756 **glacier number related values.**

| HiMAP regions | Glacier Number | | | | Glacier Area | | | |
|---------------------|----------------|------------|-------|-----------|--------------|------------|----------|-----------|
| | Surging | Surge-like | Total | Ratio (%) | Surging | Surge-like | Total | Ratio (%) |
| Karakoram | 354 | 128 | 4121 | 8.59 | 7936.12 | 1329.40 | 20103.68 | 39.48 |
| Western Pamir | 188 | 48 | 3058 | 6.15 | 2232.52 | 289.597 | 8172.64 | 27.32 |
| Western Kunlun Shan | 82 | 47 | 2508 | 3.27 | 2580.21 | 589.17 | 8466.12 | 30.48 |
| Central Tien Shan | 59 | 20 | 2248 | 2.62 | 881.61 | 305.47 | 6816.95 | 12.93 |
| Eastern Pamir | 56 | 16 | 1148 | 4.88 | 796.35 | 79.12 | 2746.47 | 29.00 |
| Tanggula Shan | 22 | 4 | 697 | 3.16 | 441.94 | 41.71 | 1937.39 | 22.81 |

| | | | | | | | | |
|----------------------------|------------|------------|--------------|-------------|-----------------|----------------|-----------------|--------------|
| Tibetan Interior Mountains | 22 | 12 | 1471 | 1.50 | 286.29 | 140.22 | 3933.48 | 7.28 |
| Northern Western Tien Shan | 21 | 6 | 1374 | 1.53 | 116.27 | 81.09 | 2502.60 | 4.65 |
| Central Himalaya | 17 | 21 | 3433 | 0.50 | 164.12 | 185.07 | 9928.72 | 1.65 |
| Eastern Kunlun Shan | 16 | 7 | 1191 | 1.34 | 458.11 | 55.38 | 2960.26 | 15.48 |
| Nyainqentanglha | 10 | 5 | 2916 | 0.34 | 119.53 | 184.79 | 7216.62 | 1.66 |
| Eastern Hindu Kush | 9 | 5 | 1279 | 0.70 | 178.18 | 77.19 | 3055.80 | 5.83 |
| Western Himalaya | 9 | 4 | 3659 | 0.25 | 110.22 | 69.41 | 8619.19 | 1.28 |
| Eastern Himalaya | 6 | 0 | 1334 | 0.45 | 94 | 0 | 3371.89 | 2.79 |
| Pamir Alay | 5 | 0 | 991 | 0.50 | 35.72 | 0 | 1957.94 | 1.82 |
| Qilian Shan | 4 | 6 | 851 | 0.47 | 35.99 | 26.40 | 1627.94 | 2.21 |
| Eastern Tibetan Mountains | 3 | 2 | 156 | 1.92 | 36.33 | 3.85 | 341.46 | 10.64 |
| Altun Shan | 2 | 3 | 156 | 1.28 | 4.13 | 3.17 | 294.95 | 1.40 |
| Eastern Tien Shan | 2 | 1 | 1243 | 0.16 | 12.03 | 2.59 | 2440.11 | 0.49 |
| Hengduan Shan | 2 | 0 | 700 | 0.29 | 26.22 | 0 | 1335.39 | 1.96 |
| Gangdise Mountains | 1 | 0 | 768 | 0.13 | 10.52 | 0 | 1339.54 | 0.79 |
| Dzhungarsky Alatau | 0 | 1 | 407 | 0 | 0 | 10.98 | 648.61 | 0 |
| Total | 890 | 336 | 35709 | 2.49 | 16556.42 | 3474.60 | 99817.72 | 16.59 |

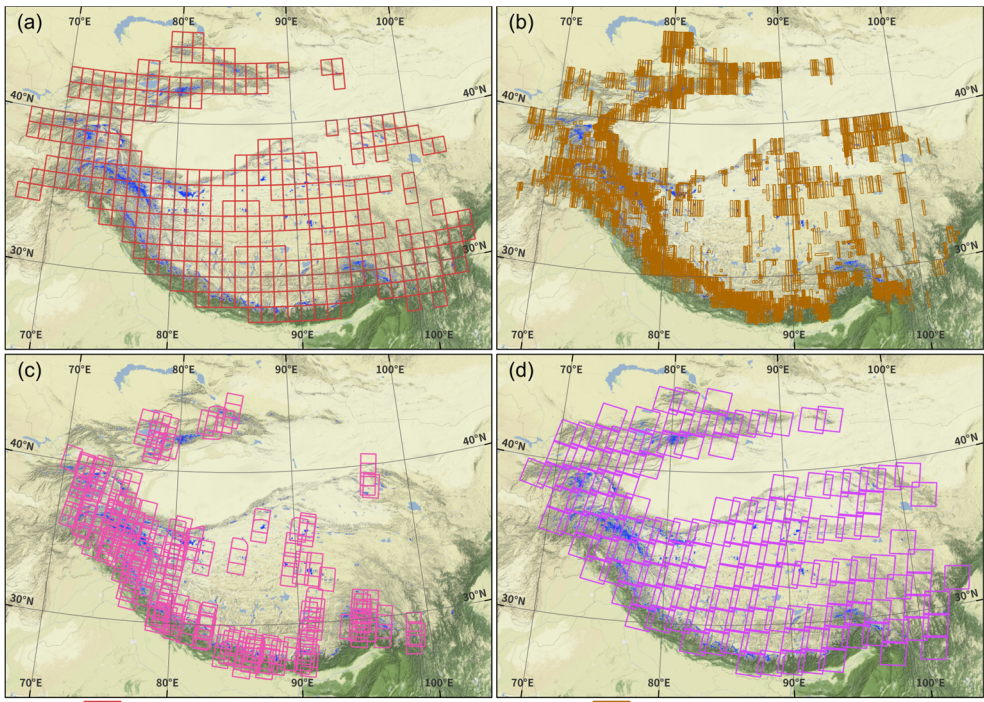
757 * The value of ratio only considered the number and area of surging glaciers.

758

759 **Table 3: Attribute information in the present surging glacier inventory.**

| Attribute | Description | Attribute | Description |
|------------------|--|------------------|--|
| Glac_ID | Glacier identifier composed by Lat/Lon | Surge_20 | Surge identified in 2000-2020 by dH |
| Area | Glacier area (km ²) | Surge_70s | Surge identified in 1970s-2000 by dH |
| Zmin | Minimum elevation of the glacier (m a.s.l) | Delta_T | Identified class of glacier terminus advance |
| Zmax | Maximum elevation of the glacier (m a.s.l) | Loop_M | Identified class of looped moraine change |
| Zmed | Median elevation of the glacier (m a.s.l) | Medial_M | Identified class of medial moraine change |
| Slope | Mean glacier surface slope (°) | False_signal | False positive signal of identification |
| Aspect | Mean glacier aspect/orientation (°) | Trib_surge | If the glacier has/is surging tributary |
| MaxL | Maximum length of glacier flow line (m) | Surge_class | Final surge identification during 1970s-2020 |
| HiMAP_region | HMA subregion that the glacier belongs to | | |

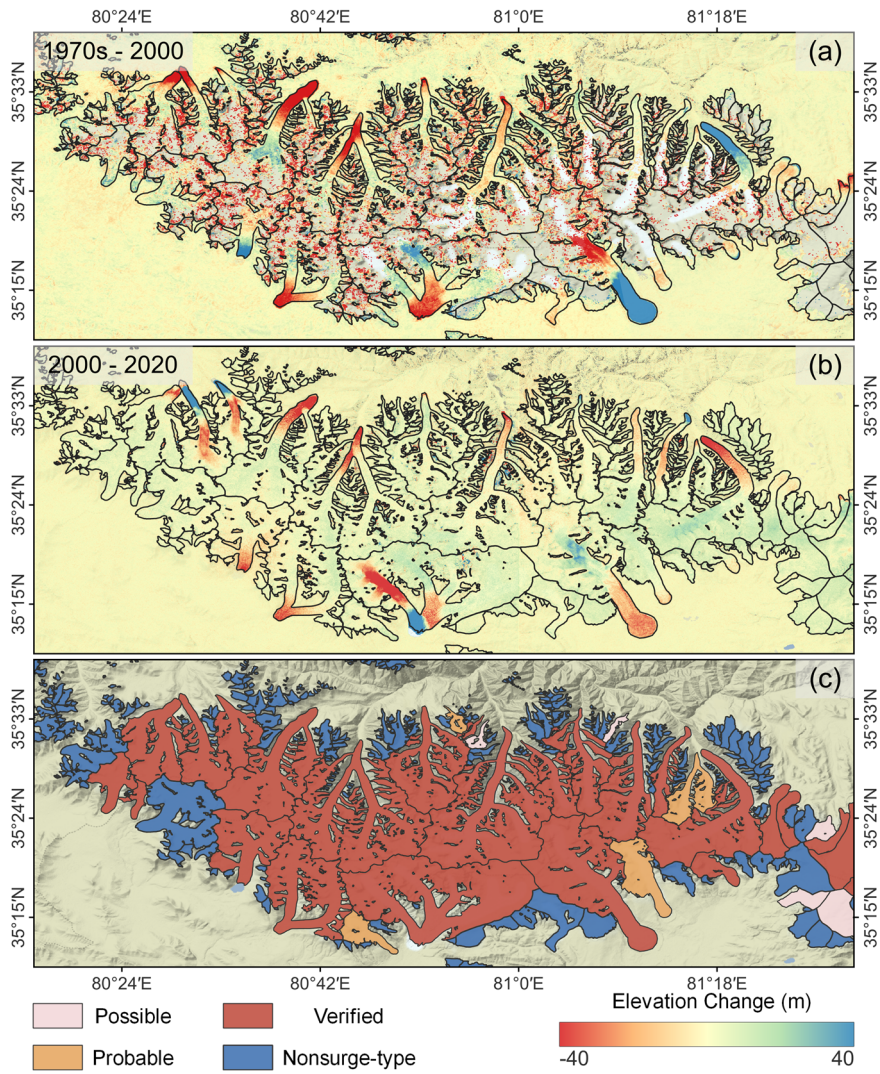
760



COP30 DEM/NASADEM Footprint (313 tiles)
 HMA8m DEM Footprint (3598 tiles)
 KH-9 DEM Footprint (238 tiles)
 Landsat images Footprint (148 frames)

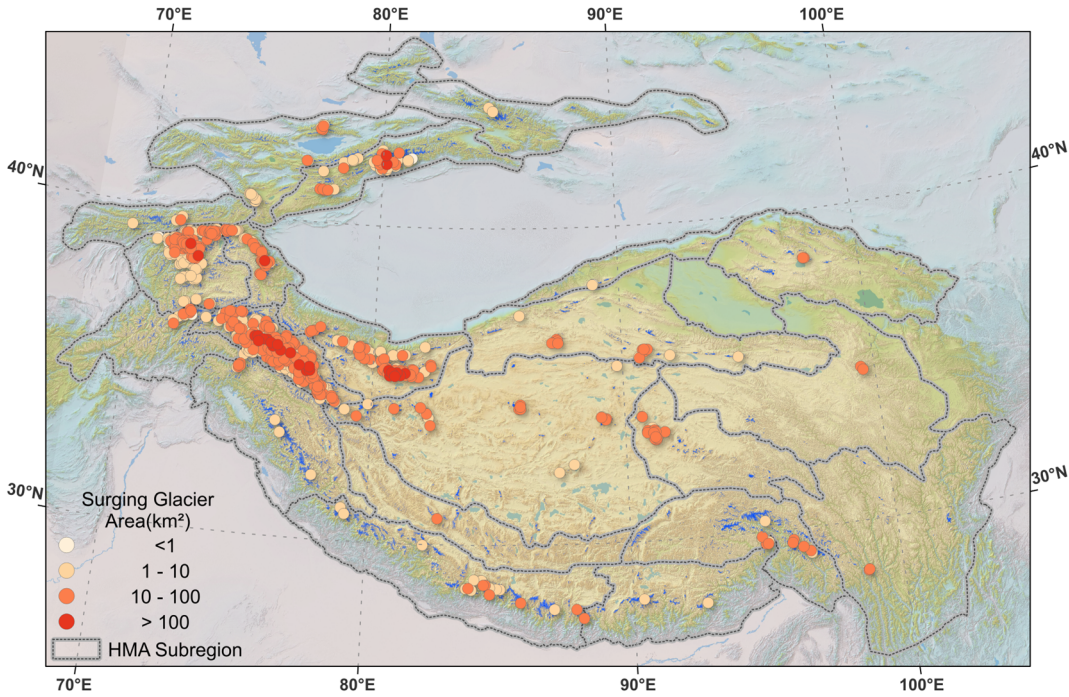
761

762 **Figure 1: Footprints of (a) COP30/NASA DEMs, (b) HMA8m DEMs, (c) KH-9 DEMs and (d) Landsat imageries that were utilized**
 763 **in this study. The background is rendered from the ESRI World Physical base map (Source: US National Park Service).**

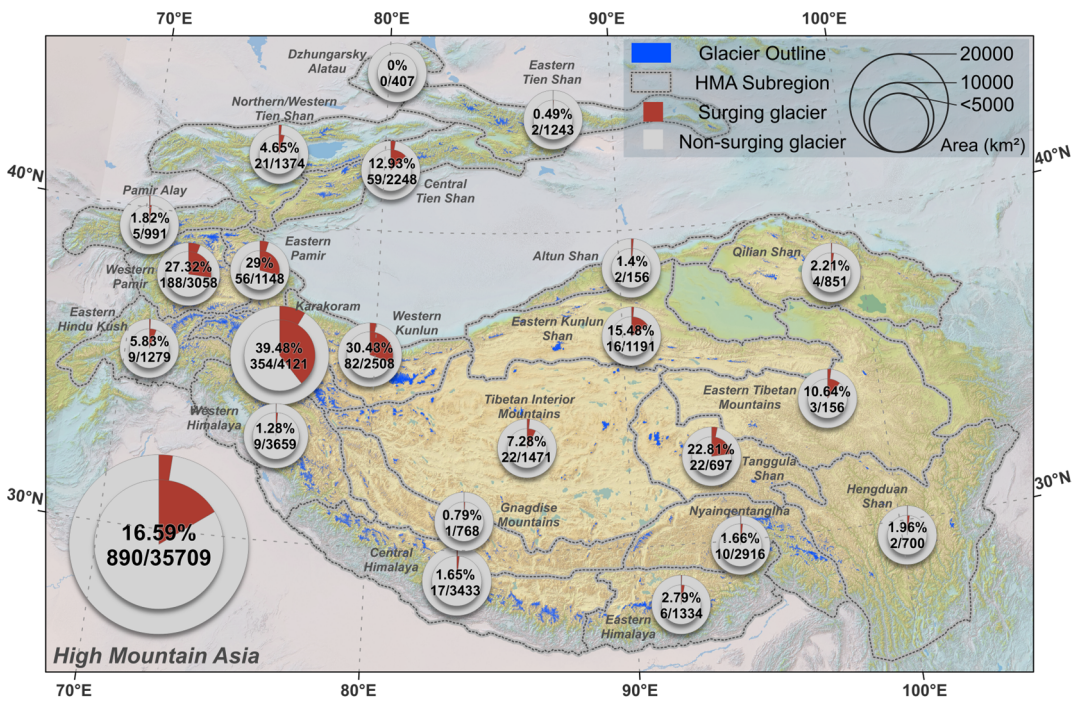


764

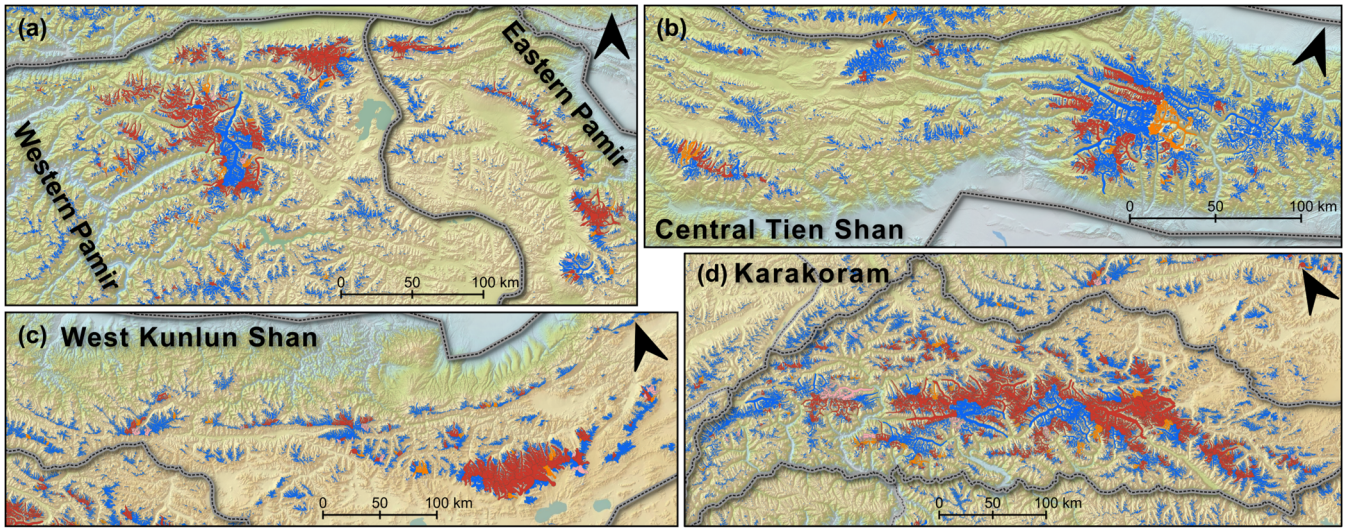
765 **Figure 2: An example of derived elevation change maps during 1970s-2000 (a) and 2000-2020 (b), and the corresponding surging**
 766 **glacier identification result (c). Black curves are glacier outlines. The background is the shaded relief of COP30 DEM (Source:**
 767 **ESA). The area is in the main massif of Western Kunlun Shan.**



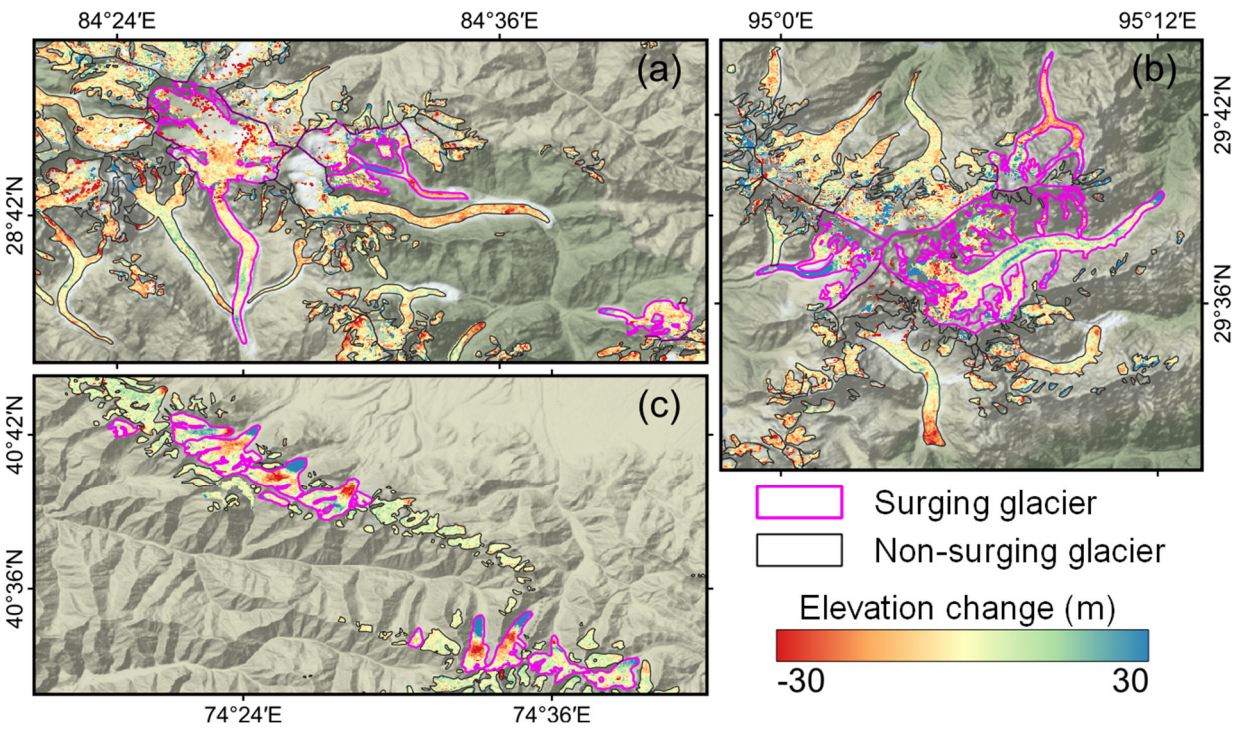
768
 769 **Figure 3: Overview of the distribution of identified surging glaciers in 22 subregions of HMA. The background is the shaded relief of**
 770 **SRTM DEM (Source: USGS).**



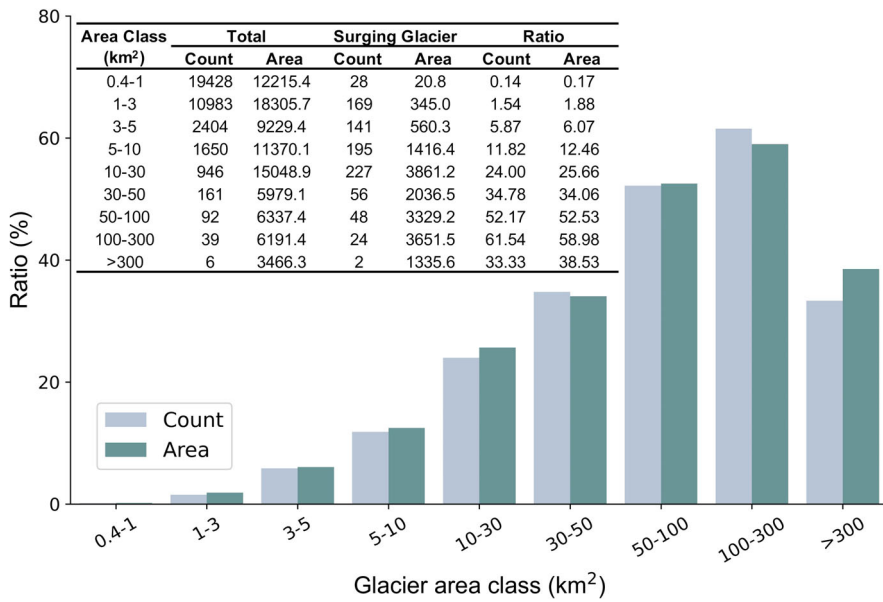
771
 772 **Figure 4: Distribution of surging glaciers in the 22 subregions of HMA. The double-level pie chart represents the ratios of surging**
 773 **glacier number and area in each subregion. The inner pie denotes the area ratio labelled by a percentage, and the outer pie denotes**
 774 **the number ratio labelled by a fraction (only considered glacier larger than 0.4 km²). The background is the shaded relief of SRTM**
 775 **DEM (Source: USGS).**



777
 778 **Figure 5: Results of surging glacier identification in the Pamirs (a), Central Tien Shan (b), West Kunlun Shan (c), and Karakoram**
 779 **(d). The background is the shaded relief of SRTM DEM (Source: USGS).**

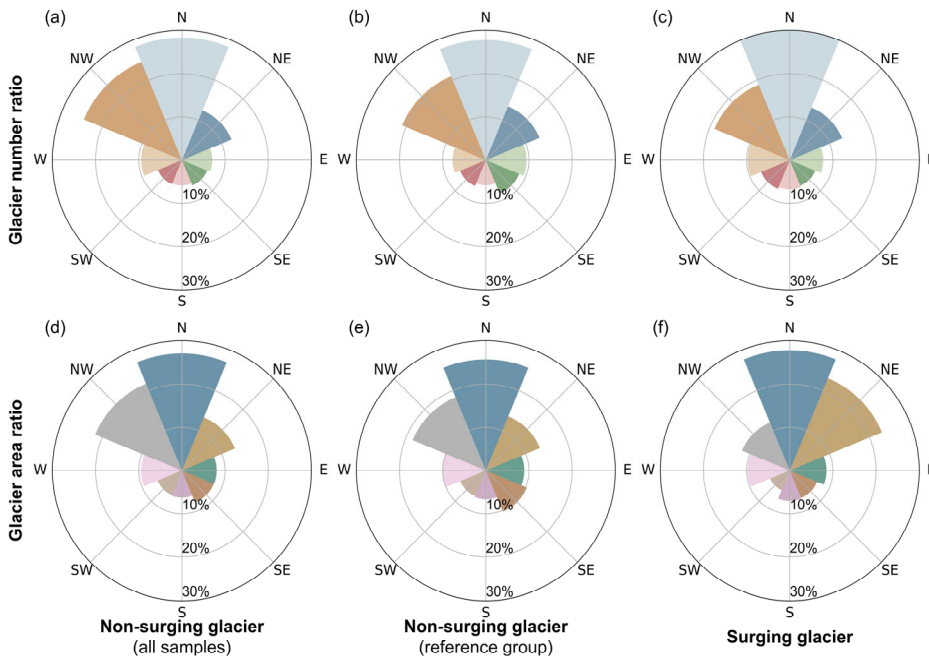


781
 782 **Figure 6: Elevation change map of identified surging glaciers samples in (a) Central Himalaya (1970s-2000), (b) Nyainqentanglha**
 783 **(1970s-2000), and (c) Northern Western Tien Shan (2000-2020). Background is the shaded relief of SRTM DEM (Source: USGS).**
 784 **Note that, surging glaciers presented in the figure were identified by combining multi-temporal elevation change and morphological**
 785 **changes.**



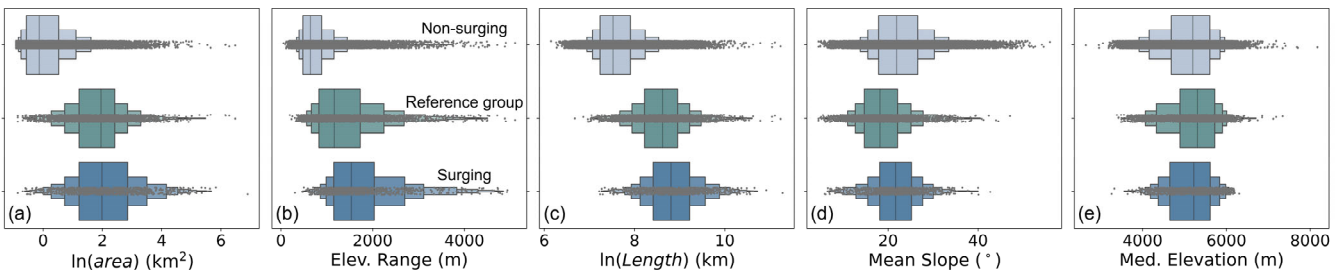
787

788 **Figure 7: The ratios of surging glacier number and area in different area classes.**



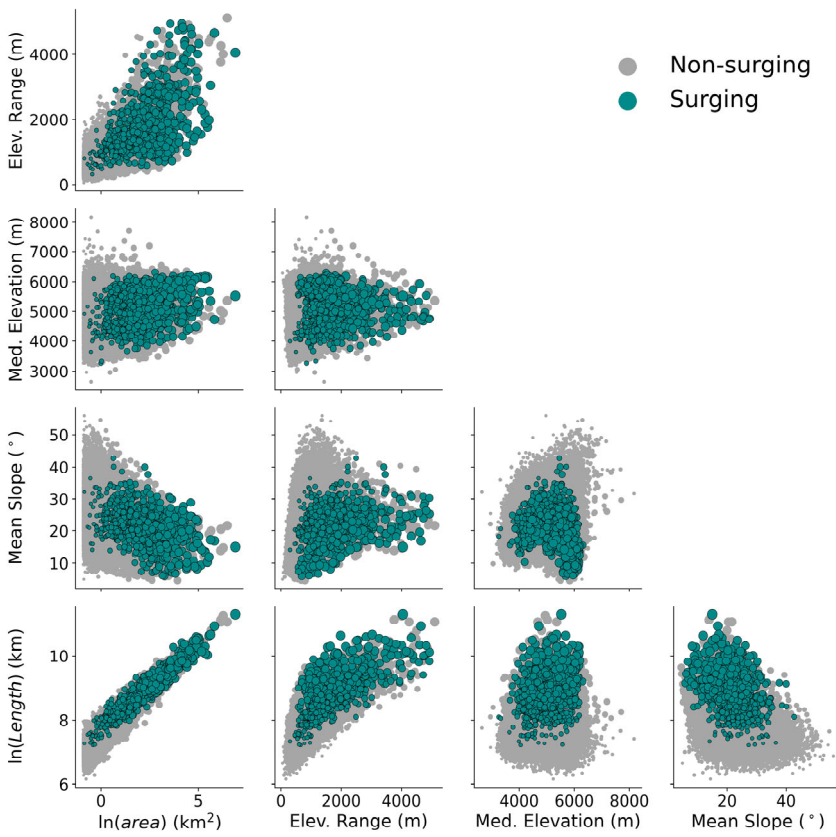
789

790 **Figure 8: The distribution of glacier number and area in eight aspects. The upper row: glacier number ratio; lower row: glacier**
 791 **area ratio. Left column: distribution of all non-surging glaciers; center column: distribution of non-surging glaciers in the reference**
 792 **group ; right column: distribution of surging glacier. Glaciers smaller than 0.4 km² were excluded in the non-surging glacier class.**



793

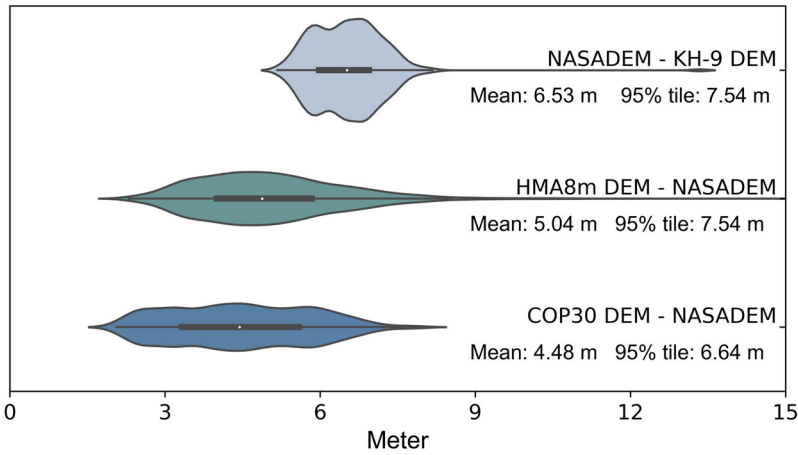
794 **Figure 9: The comparison between the boxplots of geometric properties of non-surging glaciers (top), non-surging glaciers in**
 795 **reference group (center) and surging glaciers (bottom). (a) Natural logarithm of area. (b) elevation range. (c) Natural logarithm of**
 796 **length. (d) Mean surface slope. (e) Median elevation. Glaciers smaller than 0.4 km² were excluded in the non-surging glacier class.**



797

798 **Figure 10: Bivariate scatterplots of geometric properties of non-surging and surging glaciers. The larger dots represent larger**
 799 **glaciers. Glaciers smaller than 0.4 km² were excluded in the non-surging glacier class.**

800



801

802 **Figure 11: The distribution of NMAD of elevation change observations in stable areas of all DEM differencing tiles. In each category,**
 803 **the shaded area denotes the density distribution of the NMAD of all DEM differencing tiles. The white dot denotes the median in**
 804 **each group. The thick line represents the interquartile range (IQR, i.e., 75th percentile-25th percentile) in each group. The thin line**
 805 **represents the range between the minimum value (25th percentile - 1.5IQR) and the maximum value (75th percentile + 1.5IQR).**